SSSU 114
ISSN 0140 3818

UNIVERSITY OF SOUTHAMPTON

DEPARTMENT OF SHIP SCIENCE

FACULTY OF ENGINEERING AND APPLIED SCIENCE

A STUDY INTO THE TECHNIQUES NEEDED TO ACCURATELY PREDICT SKIN FRICTION USING RANS SOLVERS WITH VALIDATION AGAINST FROUDE'S HISTORICAL FLAT PLATE EXPERIMENTAL DATA

By J.C.Date and S.R. Turnock

Ship Science Report No.114

March 1999

A Study into the Techniques Needed to Accurately Predict Skin Friction Using RANS Solvers with Validation Against Froude's Historical Flat Plate Experimental Data.

By

J.C.Date and S.R. Turnock

Ship Science Report No.114

University of Southampton

March 1999

Abstract

This report examines the conditions necessary for the accurate estimation of skin friction using a RANS code flow solver implementing the standard and RNG K-ε turbulence models. Viscous flow computations were performed for flows over various lengths of flat plate, over a range of Reynolds numbers. The results obtained were validated against Froude's original experimental data and empirical friction lines, and were found to give good agreement at all but the lowest of Reynolds numbers.

A full study was carried out to determine the necessary model and grid parameters needed in obtaining accurate viscous flow solutions. The sensitivity of the flow solutions to changes in boundary position, near wall cell spacing and the total number of grid cells were investigated.

By applying a linear least squares regression fit to the CFD data, a modified Schoenherr skin friction formula was derived, giving a formula with identical gradient and only a slight offset from the original Schoenherr line. An investigation was also carried out to determine how the effects of plate roughness could be simulated in RANS code CFD.

Table of Contents

List of Figures

List of Tables

Nomenclature

R_R	Residuary Resistance
R_F	Flat Plate Skin Friction
R_T	Total Resistance
S	Surface Area
V	Velocity
C_F	Frictional Drag Coefficient
ρ	Fluid Density
L	Flat Plate Length
ν	Fluid Kinematic Viscosity
y^+	Non-Dimensional Distance from the Wall
Δy_P	First Wall Cell Spacing
τ_w	Wall Shear Stress
Re	Reynolds Number to the Base of Length
U	Flow Velocity in the X-Direction
u^+	Non-Dimensional Flow Velocity Parallel to Wall
k	Von Karman Constant
E	Log-Layer Constant

1. Introduction

The use of CFD (Computational Fluid Dynamics) in solving ship flow problems has become common place within the marine sector over the past decade, to such an extent that in some shipyards it is now an integral part of the design spiral. It is now possible to predict many of the complex flow phenomena associated with ship flows with varying levels of accuracy and associated confidence. These include hull pressure distributions, free surface effects and viscous drag, to mention a few. However, by far the most common use for CFD is in estimating the steady viscous drag experienced by a hull form.

Traditionally Naval Architects have relied on model tests for estimating the resistance of a new ship design. CFD offers the possibility of a substantially more cost-effective route for estimating ship resistance. It may not eliminate model testing completely, but can help to reduce the total numbers of models tested. The growth of CFD has resulted in the development of a number of commercial CFD flow solvers. Consequently, viscous flow calculations are now within the reach of most Naval Architects, even in the smallest of shipyards. However, obtaining a high level of accuracy remains a considerable challenge to the Naval Architect, new to the field of CFD.

The aim of this study was to investigate the conditions necessary for accurate estimation of skin friction, at model and full scale Reynolds numbers for a simple flat plate. The flat plate geometry was chosen so that the optimum model and grid parameters for a purely viscous dominated flow could be determined, in the absence of any viscous pressure forces. A commercial Reynolds Averaged Navier Stokes (RANS) solver was used. On determining the necessary model and grid particulars, a further study was carried out to assess the effect of Reynolds number on the CFD evaluated skin friction. At low Reynolds numbers, the skin friction data was validated against Froude's original test data, and at high Reynolds numbers against empirical friction lines.

An overview of the historical background to skin friction estimation is detailed in Chapter 2. A detailed discussion of the present CFD methods used in solving viscous flows is given in Chapter 3. Chapters 4. & 5. detail the steps necessary for accurate RANS code skin friction estimation, from initial model boundary condition selection to

obtaining grid independent solutions. Chapter 6. Compares the numerical CFD results with those of Froude and those found from empirical friction lines. The conclusions drawn from the investigation are presented in Chapter 7.

2. Background to Skin Friction Prediction

Accurate estimation of a ship's total power requirement remains one of the single most important roles of a Naval Architect. It is imperative that a vessel's total resistance is established accurately early in its design, since large financial penalties are imposed on designers for failing to achieve the correct power requirement, and hence the owner specified design speed.

The total resistance of a vessel is calculated by considering the individual resistance components from which the total is made up, which can performed in a number of ways, as illustrated in Figure 1.0.

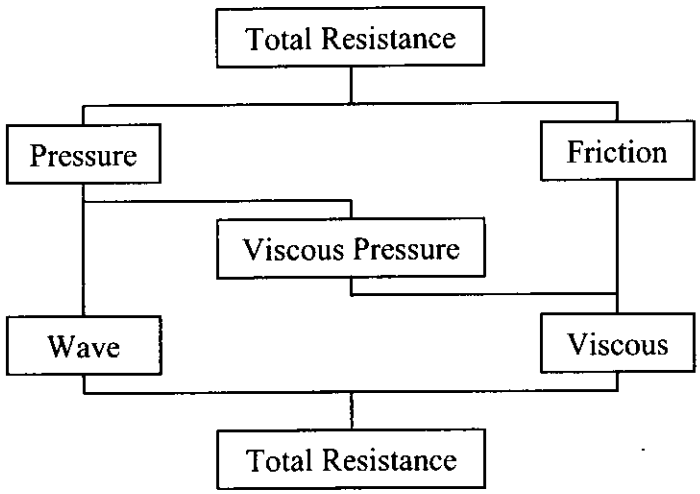

Figure 1.0 Components of Total Resistance

In ship resistance calculations, it is common to group the wavemaking, pressure and the remaining forces under the term, residuary resistance component. The total resistance experienced by a ship hull is therefore regarded as being the sum of the residuary resistance and the equivalent frictional resistance of a flat plate, as given by Equation (2.1).

$$R_T = R_R + R_F \tag{2.1}$$

For a conventional displacement vessel, the highest component of resistance is due to its skin friction. It has been shown in experiments that this accounts for approximately 80 to 85 percent of the total resistance for slow speed ships, and as much as 50 percent for fine form high speed vessels. Hence, accurate evaluation of this force is of great importance to Naval Architects.

William Froude, the father of ship resistance prediction, was the first to carry out detailed studies into ship resistance. Froude recognised the practical necessity of separating the total resistance of a ship into its separate components, based on the general law of mechanical similitude, after observing the wave patterns from geometrically similar models of different size. Froude's later work involved investigations into the governing properties of just one of the components, skin friction. His results still to this day form the basis of the empirical methods used in the prediction of skin friction.

2.1 Overview of Froude's Historical Work

After conducting experiments with models towed behind a steam launch on the river Dart, Devon, U.K. in 1868, Froude proposed that the total resistance of a vessel should be divided into two components, a skin friction component, and a residuary resistance component. Froude subsequently decided to carry out some further towing tank tests to investigate the conditions governing the skin friction component alone. These tests were carried out on vertical flat plates of varying length but fixed depth. The results of his experiments were later presented to the British Association for the Advancement of Science in 1872 [1] & 1874 [2]. The plate and towing tank particulars of Froude's tests are as follows.

Froude's Test Particulars

Plate lengths	:	1ft - 50 ft	(0.3045m-15.0m)
Plate Depth	:	19 in	(0.4826m)
Plate Thickness	:	3/16 in	(0.0048m)
Tank Length	:	278 ft	(84.73m)
Tank Width	:	36 ft	(10.97m)
Tank Depth	:	10 ft	(3.05m)
Towing Speed	:	50 - 1000 ft/min	(0.254-5.08m/s).

Full details of the apparatus and tests carried out by Froude can be found in his reports to the British Association [1]& [2].

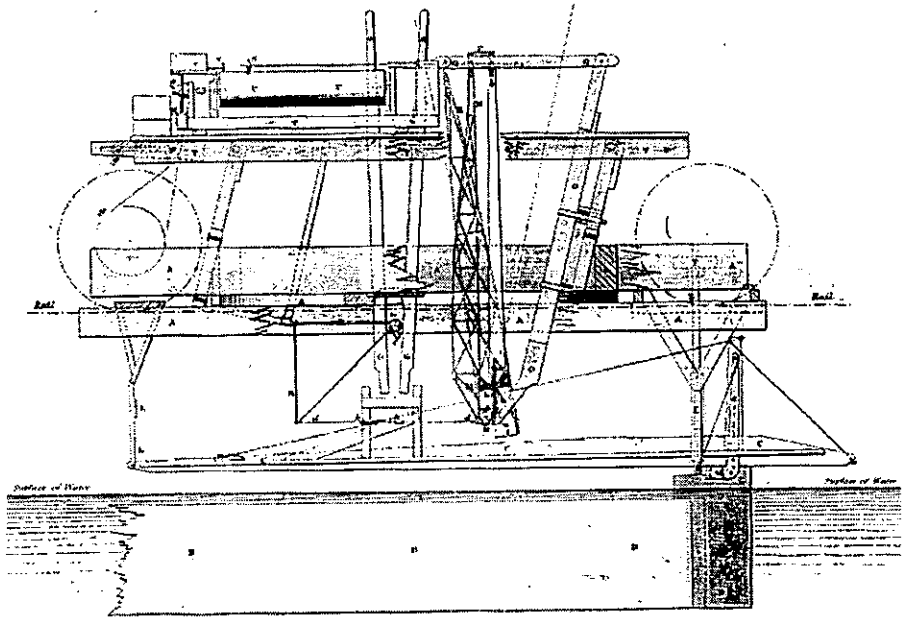

Figure 2.0 Froude's Dynamometric Apparatus (Source Ref. [1])

Figure 2.0 shows the dynamometric apparatus used by Froude in his experiments. The plates were towed, fully immersed with the upper edge approximately 40mm below the water surface in order to eliminate wave resistance, and hence the residuary resistance component previously identified by Froude. The skin friction force experienced by the plates at different speeds was recorded by means of a dynamometer. Froude's tests also attempted to identify the effect of plate surface condition on skin friction by the use of different plate surface finishes. Various sand finishes along with coatings such as varnish, paraffin, calico and tinfoil (although as he states in his report this was hard to come by!) were tested.

From his experiments, Froude concluded that at any given speed the specific resistance per unit area of surface was less for a long plate than a shorter one. In his own words he attributed this phenomena to the "Rubbing" of the portion of the plate surface which succeeds the first (i.e. the towards the after end of the plate the water had acquired a forward motion and so had a lower relative velocity). Froude gave the following empirical formula for this resistance.

$$R_F = f \cdot S \cdot V^n \tag{2.2}$$

Froude found that the coefficients of "f" and "n" in Equation (2.2) depended on the length and quality of the surface. A detailed overview of the trends Froude identified along with values of "f" and "n" for different plate surface conditions can be found in Principles of Naval Architecture [3]. Froude concluded that in order for his results to be applied to full size ships, the results would need to be extrapolated for greater lengths of plate and higher speeds. Although Froude did not derive any extrapolated data, he did suggest two methods that could be used for its derivation. He suggested that above 50 feet the decrease with increasing length of the friction per unit area would probably be small. He surmised that it would probably make very little difference to the overall estimate of total resistance whether it was taken into account or neglected over the following plate length. Froude concluded that the likely answer to this extrapolation procedure lie somewhere between these two assumptions. It was later shown by Payne [4] who reproduced Froude's curves for ships up to 500 feet in length, that Froude's conclusion was correct.

Froude did carry out some full-scale towing tests in order to obtain information to support his theories on the law of comparison, and to assist in the extrapolation of the frictional coefficient. These tests were carried out on the H.M.S Greyhound, a 172ft 6in wooden sloop which was towed by H.M.S Active at speeds up to 12.5 Knots. The results obtained by Froude were supportive of his earlier work and can be found in his report to Institute of Naval Architects [5].

2.2 Theoretical Skin Friction Evaluation

Experiments carried out by Osborne Reynolds on water flow through pipes suggested the existence of two different flow regimes, each with a different associated friction resistance law. The results of which were presented to the Royal Society in 1883 [6]. Reynolds found that these different flow conditions varied depending on the ratio of the product of local fluid velocity and the diameter of the pipe to the fluid kinematic viscosity, commonly referred to as Reynolds number. At low Reynolds numbers the flow was considered laminar (i.e. flowing in layers) and was associated with low resistance. At high Reynolds numbers the flow was regarded as turbulent (i.e. a random eddying motion) and corresponded to an increase in resistance. Modern empirical skin friction formulations assume skin friction to be a function of Reynolds number to the base of length.

Later work carried out by Blasius, Prandtl and Von Karman attempted to theoretically calculate the resistance coefficient of flat plates with respect to Reynolds number, through analytical and experimental investigations. Blasius's formulation gave the resistance of a flat plate in the laminar flow region with respect to Reynolds number [7]. Blasius showed that his calculated resistance values were close to the results found by Froude at low Reynolds numbers.

Prandtl and Von Karman's formulation however, determined the resistance of a flat plate in the turbulent flow region based on a $^1/_7{}^{th}$ power law boundary layer velocity distribution [8]. This formulation found good agreement with Froude's findings at the high Reynolds Numbers. The laminar and turbulent resistance equations derived by Blasius, Prandtl and Von Karman are as follows.

Laminar (Blasius)

$$C_F = \frac{R_F}{1/2 \cdot \rho \cdot S \cdot V^2} = 1.327(\mathrm{Re})^{-1/2} \qquad \mathrm{Re} < 5 \times 10^5 \tag{2.3}$$

Turbulent (Prandtl & Von Karman)

$$C_F = \frac{R_F}{1/2 \cdot \rho \cdot S \cdot V^2} = 0.072(\mathrm{Re})^{-1/5} \qquad 5 \times 10^5 < \mathrm{Re} < 1 \times 10^7 \tag{2.4}$$

These formulae give good approximations of the resistance coefficients for flat plates with either laminar or turbulent flow conditions. However, Prandtl identified that the Reynolds numbers occurring in practical applications generally exceeded the range of validity of $^1/_7{}^{th}$ power law Equation (2.4) and sort to derive a resistance formula that would be valid at much higher Reynolds numbers. Prandtl later derived a skin friction formula based on the universal logarithmic boundary layer velocity profile, which could be extrapolated up to arbitrary large Reynolds numbers [9]. The form of this skin friction equation is shown below.

Turbulent (Prandtl)

$$\frac{1}{\sqrt{C_F}} = A + B \log_{10}(\mathrm{Re} \cdot C_F) \tag{2.5}$$

The constants A & B in Equation (2.5) were determined by fitting the equation to available experimental test data. Following the publication of this formula, Schoenherr re-plotted all the available experimental flat plate data to obtain the constants A & B to give Equation (2.6) [10]. This formula is still frequently used today in calculating skin friction of ship hulls.

Turbulent (Schoenherr)

$$\frac{1}{\sqrt{C_F}} = 4.13 \cdot \log_{10}(\mathrm{Re} \cdot C_F) \tag{2.6}$$

All the formulas given above make good approximations for flows in either the laminar or the turbulent flow regions, but do not account for transition between the two. The transition between the two different flow phenomena is not a simple one, since it does not occur simultaneously over the whole plate, see Figure 3.0.

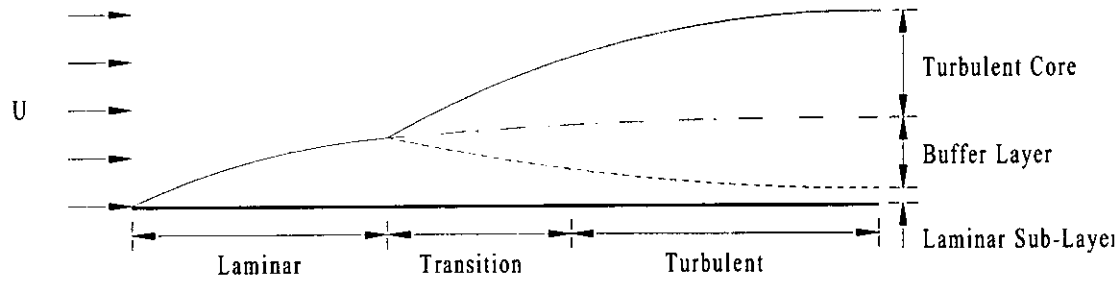

Figure 3.0 Flat Plate Boundary Layer Transition

The transition on a flat plate occurs when the local Reynolds number reaches a critical value. As the velocity, and hence the Reynolds number increases, the point of transition along the plate surface moves forward towards the leading edge so that the local Reynolds number remains equal to the critical. The local Reynolds number is defined with respect to the distance from the leading edge of the plate to the point of transition. Therefore, for any flat plate flow there will be a small region of Laminar flow followed by a turbulent region, and hence two regions with different resistance characteristics.

2.3 ITTC Correlation Line Procedures

As a result of the growing interest in the field of ship skin friction evaluation, the International Conference of Ship Tank Superintendents (ICSTS) was founded in 1932, to provide a discussion forum for those working in the field of ship resistance. The ICSTS later changed its name to the International Towing Tank Committee (ITTC) in 1957. The aim of the organisation was to arrive at a standard procedure for predicting ship resistance based on the model extrapolation method put forward by Froude, and using the resistance coefficients derived by him and later researchers such as Schoenherr and Hughes. A Skin Friction Committee was set up within the ITTC to carry out further research into a turbulent skin friction line, similar to those of Prandtl which could be used in both model and ship skin friction prediction based on Reynolds number. Following further research and analysis of previous data, a skin friction preliminary model-ship correlation line was established at the 1957 Madrid ITTC conference based on an approximated explicit form of Schoenherr original formula, see Equation (2.7) [11]. This model-ship correlation line is still used today in model-ship resistance calculations. It must be stressed that the ITTC 1957 Equation is a model-ship correlation line, and not a frictional resistance line similar to those derived by Blasius and Prandtl. It is not meant to represent the frictional resistance of plane or curved surfaces, only to serve as an extrapolation line for the calculation of skin friction from model to ship scale. This is because it is essentially a modified form of the Schoenherr formula, with a steeper slope at low Reynolds numbers, to give better correlation between the skin friction estimates of small and large models.

ITTC 1957 Model-Ship Correlation Line

$$C_F = \frac{0.075}{[\log_{10} \mathrm{Re} - 2]^2} \tag{2.7}$$

3. Present CFD Methods Used in Solving the Skin Friction Problem

Although the fundamental governing equations of fluid flows were derived early in the nineteenth century by the early fluid dynamicists, Navier and Stokes, solutions to their equations for practical fluid problems remained elusive for all but the simplest of fluid flows, until the advent of the digital computer.

The field commonly referred to as Computational Fluid Dynamics or CFD, which involves finding numerical solutions to the equations derived by Navier and Stokes has seen rapid advances in the past three decades. These advances as one would expect, have occurred in parallel with advances in computer technology. Increased processor speed, memory size and the use of better solution algorithms have allowed even more complex fluid flow problems to be solved, than was imaginable on the first digital computers. Much of the pioneering research and development in CFD came from the aircraft industry in the early years, with their vast resources and budgets. However, with the ever-decreasing cost of computer hardware, CFD has now became a viable and fast growing research tool across all engineering disciplines. The marine industry was slow at first to recognise the potentials benefits of CFD as a design tool, mainly as result of the high overheads associated with such a specialised activity, and the inherent flow modelling difficulties associated with unsteadiness and free surface effects. However, many shipbuilding companies are now carrying out detailed CFD studies themselves or via third parties specialised in the field of CFD, as identified by Bertram [12].

CFD is commonly implemented within the design spiral where it is used as an optimisation tool, allowing parametric studies to be carried out on conceptual hull designs before deciding on a final design, see Martinelli [13]& Marzi [14]. Although model tests are usually carried out on final designs to confirm the CFD results, the use of CFD to compare designs is significantly more cost effective than carrying out individual model tests. CFD also has the advantage that it allows innovation in design, hence more radical designs can be tested which might otherwise have been discounted in say, model tests in favour of more traditional designs due to model and tank costs. Of all the uses of CFD in ship design, ship resistance is by far the most common application. At present, CFD solutions are limited to flows at Reynolds numbers much lower than ship scale, due to problems associated with grid resolution and turbulence modelling. Hence, CFD ship flow investigations are generally conducted at model scale

only. With current technology, it is reported that the accuracy of resistance calculations lies somewhere between 2-3% of those found by experiment, see 21st ITTC [15]. It is widely hoped within the marine industry that these errors will be reduced further, to the extent that CFD can replace the need for model testing, although this is widely debated.

3.1 NSS, LES & RANS Solvers

The advances briefly discussed above allow solutions to the complex viscous incompressible flows associated with marine craft to be solved. Solutions to the Navier Stokes equations presently fall into three categories, full Navier Stokes Solutions (NSS) or Direct Navier Stokes (DNS), Large Eddy Simulations (LES) and Reynolds Averaged Solutions (RANS).

The use of NSS codes in ship resistance calculations is uncommon in the marine sector, as a great deal of research in this field is still needed. NSS for fully turbulent flows at high Reynolds numbers such as ship flows have yet to be obtained and await major advances in computational hardware, allowing all the individual eddies to be resolved down to the smallest length scales. A detailed discussion of NSS solvers and the future of CFD are presented by Anderson [16]. Although NSS solvers are presently limited to solving low Reynolds flows, they are playing a major role in RANS code turbulence model development.

Like NSS codes the use of LES solvers is rare and mainly the preserve of the CFD researcher. These solvers are similar to NSS codes in that they resolve individual eddies but only of large scale, requiring a sub-grid scale model to represent the small scale eddies. Although only the large scale eddies are resolved individually, this still requires the use of extremely fine grids, making solutions expensive and demanding on present computer resources. However, it is widely believed that LES codes will become the new standard in calculating turbulent flows with ever increasing computing power, long before NSS solvers.

RANS code flow solvers are by far the most commonly used CFD tool for solving viscous ship flow problems at the present time. RANS solvers take the fundamental Navier Stokes equations and average them over a period of time, introducing Reynolds stresses which require closure for solution, see Equation (3.1). Closure is provided by way of turbulence model, which predicts these Reynolds stresses,

represented by the last term on the left-hand side of Equation (3.1) and calculated using the Boussinesq assumption given by Equation (3.3).

Steady State Incompressible Reynolds-Averaged Navier-Stokes Equation

$$U_j \cdot \frac{\partial U_i}{\partial x_j} + \frac{\partial P}{\partial x_i} - \frac{\partial}{\partial x_j} \cdot \left(\nu \cdot \frac{\partial U_i}{\partial x_j} \right) - \frac{\partial \tau_{ij}}{\partial x_j} = 0 \tag{3.1}$$

Continuity Equation

$$\frac{\partial U_i}{\partial x_i} = 0 \tag{3.2}$$

Boussinesq Reynolds-Stress Equation

$$\tau_{ij} = \nu_t \cdot \left(\frac{\partial U_i}{\partial x_j} + \frac{\partial U_j}{\partial x_i} \right) \tag{3.3}$$

A number of turbulence models have been developed for use within RANS codes, all of which vary in both complexity and suitability to specific flow problems. The use of RANS codes in solving the viscous flow problems associated with ship flows has been widely documented, however the accuracy of the results obtained are the subject of much discussion. The accuracy of RANS code solutions are limited mainly by the lack of robust turbulence models capable of solving a wide range of flow problems.

Often the validity of CFD results are lost amongst many colourful and impressive flow visualisation outputs. This report will outline many of the difficulties associated with modelling viscous flow problems, and obtaining accurate flow solutions using a commercial RANS code. The study will be focused on investigating the flow over a simple flat plate, in the context of solving the ship skin friction problem.

3.2 CFD Validation

The wide spread use of CFD in the marine industry has raised the question of code validation. This has brought into question the development of quality standards, in an attempt to improve confidence within the industry and to satisfy the requirements of regulatory bodies. The major emphasis of such standards is to insure that a known level of accuracy is achieved by flow solvers. In terms of validation, it is impossible to assess

the prediction performance of a complex CFD code by any means other than by comparison with experimental work. Hence, ship model test data and full size ship trails data are commonly used as benchmarks for assessing the validity of CFD flow solutions. Closed form analytical solutions are also used, but are restricted in their application to practical flow problems.

Recognising the need for validation in the marine CFD sector, the International Towing Tank Conference (ITTC) in conjunction with the American Society of Mechanical Engineers (ASME) has been at the forefront in establishing guidelines and standards. In turn ensuring continuing high standards in CFD. The proposed standards address all aspects of CFD, not just accuracy of solutions. A detailed résumé of the proposed guidelines can be found in the proceedings of ITTC (1996) [15]. The ITTC guidelines for validation of code solutions are based on those detailed in the policy statement of the ASME, which require authors to address a number of criteria for assessing numerical uncertainty. Although general validation of a code is still the responsibility of the fluid dynamicist, or programmer, the final user must appreciate the need for careful studies in order to assess the validity of a model and its solutions. Detailed validation studies as required by the ITTC will be applied to the flat plate solutions presented in this report.

4. RANS Code Skin Friction Modelling

As mentioned previously a considerable amount of research has been conducted in the field of skin friction estimation using CFD. However, much of this research has been conducted on actual ship hull forms or bodies of revolution, which experience both pressure and viscous forces. It was decided that a flat plate resistance study would be carried out to determine the model and grid parameters necessary for accurate viscous flow modelling, in the absence of these large viscous pressure forces. With the viscous friction forces accounting for a substantial proportion of a vessel's resistance, and requiring the most critical grid particulars, this study allowed the model to be optimally refined for accurate skin friction estimation. It is hoped that the results from this general study will provide the Naval Architect with the necessary information to produce models with the required grid parameters for accurate skin friction evaluation. The low Reynolds number flat plates modelled had exactly the same dimensions as the plates

tested by Froude, allowing validation against the data presented in his reports to the British Association [1] & [2].

4.1 RANS Flow Solver

The RANS flow solver used for the skin friction calculations within this report was CFX-4.2, a structured multi-block, finite volume flow code produced by AEA Technologies [18]. The multi-block grids were produced using Meshbuild a sub-program within CFX-4.2. Various differencing schemes were used on the convection terms, from first order to third order, these will be discussed in greater detail later in the report. Velocity-Pressure coupling was resolved using the PISO (Pressure Implicit with Splitting Operators) iterative solution strategy. The linearised difference equations were solved using the Algebraic Multi-Grid (AMG) solution method. Two different high Reynolds number turbulence models were tested, standard K-ε and RNG K-ε. The convergence criteria for all runs was based on the sum of the absolute mass residuals reaching 1.0×10^{-6}.

4.2 Flat Plate Grid Topology

Many different plate geometries were tested by Froude, varying in length, surface condition and leading and trailing edge shape. The varying leading and trailing edge shapes and surface finishes are illustrated in Froude's reports to the Royal Association [1] & [2]. It was decided that only Froude's plates having fine leading and trailing edges would be modelled and compared with his findings, since these plates would experience nominal viscous pressure forces.

Initially a full three-dimensional model was going to be used to model the various lengths of plate. This would allow the very small amount of resistance contributed by the upper and lower edges of the plate to be considered along with the effects of aspect ratio. However, this posed serious gridding problems when using the structured multi-block method used in CFX-4.2. In two-dimensions, it is extremely easy to produce a simple H-Grid for the problem, using three blocks. However, problems arise when the model is extend in three-dimensions, since it becomes extremely difficult to grid effectively around the sharp leading and trailing edges of the plate.

Ideas such as the use of C-Grids around the leading and trailing edges or the use of a finite thickness leading and trailing edge were considered as solutions to the

problem. The use of a C-Grid was discounted because of its associated poor grid quality at the leading and trailing edges, which would have caused greater inaccuracies in solution than if the plate had been modelled in two-dimensions ignoring the edge effects.

The best solution to the three-dimensional problem was to use a finite thickness leading and trailing edge. This method produced very thin blocks upstream and downstream of the plate, making the blocking above and below the plate a trivial matter. This gridding method was therefore implemented, but had little success in gaining converged solutions. The finite thickness leading and trailing edges were made 0.5mm thick, producing small faces with a negligible contribution to the overall drag of the plate. The grid propagation used on the neighbouring blocks in the X, Y & Z directions were set so that the last cell matched the cell size of the small upstream and downstream blocks. After much grid refinement and solver adjustments, it was found that a converged solution was unobtainable for this model. Subsequent two-dimensional work suggested that this convergence problem, might have been as a result of placing too small or too many cells within the laminar sub-layer and is discussed in detail in Chapter 5.2. It was, therefore decided not to pursue this problem any further, and to model the plates in two-dimensions, since the resistance contribution from the small area, on the upper and lower edges of the plate account for less than 0.5% of the total area, and hence the resistance.

The plates were therefore modelled using a simple H-Grid made up of three blocks as shown in Figure 4.0. Using the blocking method shown, a highly regular orthogonal grid can be produced on subsequent gridding of the blocks. This is in fact, the best form of grid for obtaining accurate CFD solutions, however such regular grids are rarely produced when complex hull forms of actual ships are considered. Regular grids have the advantage that they allow the flow to be aligned with the grid lines, reducing the possibility of false diffusion, which can arise from flow not being suitably aligned with the grid. A comprehensive study into the effect of false diffusion on flow solutions for various differencing schemes is discussed by Versteeg & Malalasekera [17]. The thickness of all blocks in the Z direction was 0.4826m, the same as the depth of the plates tested by Froude. The block dimensions in the X & Y directions were determined by means of a boundary positioning sensitivity study and will be discussed in Chapter 4.4.

4.3 CFD Model Boundary Conditions

It is necessary in all CFD problems to define the initial and boundary conditions that physically describe the problem to be solved. The selection of these boundary conditions is fundamental to obtaining accurate flow solutions. Since the flow solutions are essentially obtained from interpolation on the boundary condition values, the use of unrealistic and badly posed boundary conditions can lead to spurious and incorrect flow solutions, not to mention rapid solver divergence. Therefore, a well-posed CFD problem is one whose solution depends in a continuous way on the initial boundary conditions. There are a number of boundary condition combinations that could be applied to the simple problem of viscous flow over a flat plate, leading to a valid flow solution. However, the selection of certain boundary conditions can result in excessive computational effort being needed to solve a problem.

In this two-dimensional skin friction investigation, it was only necessary to model one side of the plate. Halving the problem and defining a symmetry plane reduces the number of cells and hence the time needed to solve the problem with no compromise in accuracy. Figure 4.0 shows the boundary conditions used.

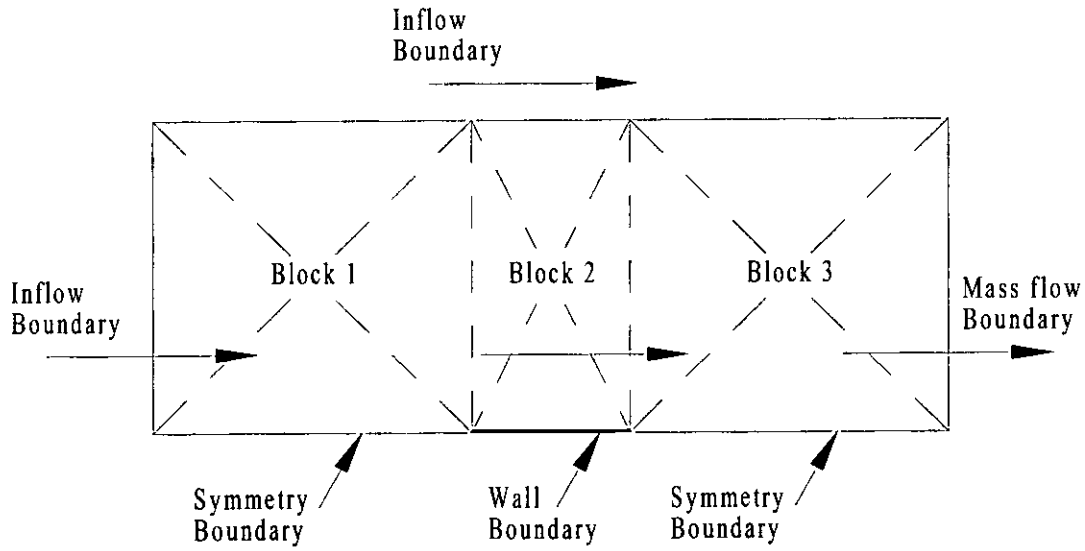

Figure 4.0 Flat Plate Model Boundary Conditions

The plate itself, was modelled as a wall with a no-slip condition applied to it, i.e. U = V= 0 on the wall. The lower faces of the upstream and downstream blocks 1 & 2 were modelled as symmetry planes. The left-hand face on Block 1 was modelled as an inlet with the flow velocity set to the corresponding plate velocity. The right hand face of Block 3 was modelled as a mass flow boundary outlet. The upper three faces of all three

Blocks were modelled as inlets with the same corresponding plate velocity as the upstream inlet. The inlet turbulence parameters K & ε were both set to zero, i.e. the free stream undisturbed flow condition. Usually these should be set according to the measured values found from experiments, however this is not always possible and assumed values must be used. Usually, if the upstream inlet boundary is placed far enough upstream, the choice of K & ε becomes less critical, since the flow variables K & ε tend to dissipate down to suitable values. An example of the command file used to define the solution parameters and the boundary conditions can be found in Appendix.

These boundary conditions were chosen because they were found to give the quickest flow solutions for similar modelled flows carried out using CFX. The upper boundary condition could well have been set as a symmetry plane or a constant pressure boundary, likewise the upstream and downstream boundaries could have also been defined as constant pressure boundaries. The use of an upper pressure boundary condition, has been shown in previous investigations as a poor choice, because it needs to be placed at excessive distances away from the lower wall to ensure no flow crosses through it. The selection of a boundary condition such as this would obviously increase the size of the grid needed to model the flow effectively and hence increase solution time.

4.4 CFD Model Boundary Positioning

Whilst the selection of the boundary conditions is of utmost importance, their positioning, can be equally critical. It is important that all boundaries are positioned to ensure that they have no effect on the flow solution obtained. With regard to the CFD model of the Froude's plates, a study was carried out into the minimum distance needed in positioning the inlet, outlet and upper inlet boundaries. It is important in any CFD study, where high accuracy results are required, for a sensitivity study to be carried out to demonstrate that the interior flow solution is unaffected by the location of the model boundaries.

In CFD flow solutions, by far the most important boundary location is the outlet mass flow boundary. All outlets should be placed far enough downstream, to ensure that the fluid flow is fully developed (i.e. zero flow variable gradients in the flow direction). The positioning of an outlet too close to an area with a flow disturbance may result in solution errors, since the assumed outlet condition of zero flow gradient does not hold.

With regard to bluff body flows, it has been shown that there will also be an area of reversed flow downstream. This reversed flow would therefore contradict the outlet boundary condition of outward flow if the outlet was placed too close to the body. It must also be remembered that it is not good practice to place boundaries at excessive distances from the body. This wastes valuable computational resources, which could be put to better use in resolving areas with high flow gradients.

The boundary position sensitivity study carried out on the Froude's plate model, involved moving one of the outer boundaries until convergence on the plate skin friction was obtained, whilst the remaining two boundaries were held fixed. This was done in turn for all three outer boundaries. The positioning of the boundaries was based on the plate length and ranged from L/8 to 4L. All the grids used in this sensitivity study were made up of a uniform distribution of cells in the X & Y directions of fixed size regardless of the boundary position. This ensured that any variations in results, were due to the boundary positioning, not cell size or propagation.

This convergence study was carried out on the longest plate tested by Froude of 50ft (15.24m) at the maximum test speed of 5.08m/s, the condition of maximum turbulence. A third order differencing scheme was used on the flow variables and the standard K-ε turbulence model was employed. The results from the study are shown in Table 1.0,Table 2.0 & Table 3.0. For the inlet and outlet parametric studies, the upper inlet boundary was positioned at a distance 2L above the plate. For the upper inlet boundary parametric study, the inlet and outlets were positioned at a distance of L upstream and downstream.

Outlet Position	C_F (x 10^{-3})	No. Iterations	CPU Time (Sec)	No. Cells
L/8	2.211	191	515	6800
L/4	2.210	171	503	7200
L/2	2.210	172	583	8000
L	2.209	165	706	9600
2L	2.209	187	1141	12800
4L	2.209	227	2217	19200

Table 1.0 Outlet Boundary Position

Inlet Position	C_F (x 10^{-3})	No. Iterations	CPU Time (Sec)	No. Cells
L/8	2.213	176	450	6800
L/4	2.211	170	463	7200
L/2	2.209	176	581	8000
L	2.209	165	656	9600
2L	2.209	172	980	12800
4L	2.209	166	1666	19200

Table 2.0 Inlet Boundary Position

Upper Inlet Position	C_F (x 10^{-3})	No. Iterations	CPU Time (Sec)	No. Cells
L/4	2.217	96	31	1200
L/2	2.212	99	69	2400
L	2.210	111	183	4800
2L	2.209	165	706	9200
4L	2.209	364	4322	19200

Table 3.0 Upper Inlet Boundary Position

It can be seen from the data in Table 1.0,Table 2.0 & Table 3.0 that convergence on skin friction has been reached on all of the boundary condition positions. Comparing Table 1.0 with Table 2.0 it is obvious that the solution to the flow problem is more sensitive to the downstream outlet boundary condition than the upstream inlet condition. In fact the upstream inlet can be placed as close as half the plate length upstream of the plate without affecting the flow solution, whereas the outlet mass flow boundary must be placed at least one plate length downstream. It is quite surprising to note, from the data in Table 2.0 that the upper inlet needs to be placed at least two plate lengths above the plate before the solution becomes boundary independent.

It should be noted from this study that the number of iterations taken in obtaining a solution are generally unaffected by the boundary position once convergence has been reached. This is because the additional number of cells resulting form the increased size of the flow domain have no effect on the flow, having the same transport properties at the outer cells of the previously converged solution. Additional cells merely serve to increase the number of equations to be solved and hence the time for solution.

Based on the results found in this study it was decided that all the inlet and outlet boundaries would be placed at a distance 2L from the plate to ensure boundary independence.

5. Grid Parameters and Grid Independence

Before a CFD solution can be regarded as accurate and valid, it must demonstrate that it is independent of the grid used for solution. By virtue of the fact that the governing equations are approximated, by the use of a finite number of grid cells in the representation of continuously varying flow field, it is not surprising that flow solutions are sensitive to the number of grid points. It is therefore necessary to demonstrate for a particular solution, that grid independence has been achieved. A grid independence study involves carrying out solutions on the CFD model, with successively refined grids of reduced cell size, until the flow-field variables become independent of the cell size, distribution and number. When an asymptotic limit is reached for a specific solution, the solution can be considered as grid independent (i.e. its solution is independent of the coarseness of the grid). The process of finding a grid independent solution can be a complex one, especially when three-dimensional grids are considered, as the grid proprieties in each dimension are often interrelated with regard to the flow-field variables.

The degree of grid independence for a particular CFD model should however, be related to the degree of accuracy needed in the final solution. The difference between a fully grid independent solution and an error of 1% in the solution, can often be as a result of a 10 fold increase in the number of cells. Excepting a possible 1% error can therefore save time and money when extreme accuracy is not necessary.

5.1 Turbulence and Near Wall Grids

The use of wall function turbulence models in formulating the closure to the Navier-Stokes equations place specific requirements on the grids used in solving turbulent flow problems. When considering turbulent near wall flows, the most critical grid parameter is the near wall grid spacing. It is of paramount importance that near wall grid spacing is selected in accordance with the requirements of the turbulence model. The selection of the right turbulence model and associated near wall cell spacing is however, dependent on the problem's turbulent flow characteristics and hence the Reynolds number. A detailed explanation of turbulence models and modelling is beyond the scope of this report, however, the implications on the near wall grid will be discussed in detail. Explanations of turbulence modelling and the use of RANS code turbulence models can be found in most CFD texts such as Versteeg & Malalasekera [17].

From experimental work, it is known that near wall flows have a characteristic multi-layered structure within the boundary layer. This consists of a laminar sub-layer (viscous force dominated) close to wall followed by a buffer layer (viscous and turbulent forces of similar magnitude) and then an outer turbulent core (turbulent stress force dominated), see Figure 3.0. Direct methods of resolving the turbulent eddies within this boundary layer require extremely fine grids down to the wall through the laminar sub-layer, which is computationally intensive and very costly. However, most RANS code turbulence models get round this problem by employing wall functions based on the universal law of the wall. The use of wall functions avoids the need for fine grids in the boundary layer by making use of empirical fits within this region. Both the turbulence models investigated in this report make use of this wall function approach.

When dealing with near wall flows, positions and velocities within the boundary layer are usually considered in a non-dimensional form known as y^+ & u^+. y^+ is a form of non-dimensional local Reynolds number with length scale in the direction perpendicular to the wall and is represented by Equation (5.1) below .

$$y^+ = \frac{\Delta y_P}{\nu} \cdot \sqrt{\frac{\tau_w}{\rho}} \tag{5.1}$$

u^+ is a non-dimensional form of velocity at a distance away from a wall and is represented by Equation (5.2) below.

$$u^+ = \frac{U}{\sqrt{\frac{\tau_w}{\rho}}} \tag{5.2}$$

Non-Dimensional analysis and experimental work has shown that the specific flow structures within the boundary layer lie within strict bounds of y^+ and these are used in the formulation of wall functions. Positions within the boundary layer in which $y^+ \leq 11.63$ are regarded as being laminar in structure, and positions where $y^+ \geq 11.63$ are considered as being turbulent. It has been shown that within these two regions two different functional relationships exist between y^+ and u^+, given by the following equations.

Laminar Linear Sub-Layer Region

$$u^+ = y^+ \tag{5.3}$$

Turbulent Log-Law Region

$$u^+ = \frac{1}{k} \cdot \ln(Ey^+) \tag{5.4}$$

The constants in Equation (5.4) are determined by experiment. For hydraulically smooth walls, the Von Karman constant $k = 0.4$ and the log-layer constant $E = 9.793$. Roughness can be simulated by increasing the value of E. The buffer layer cross over value of 11.63 is found by finding the intersection of the linear laminar sub-layer profile (5.3) and the log-law turbulent profile (5.4).

Making the best use of this wall function approach requires the correct positioning of cells within the boundary layer. Usually, in wall function CFD, turbulent calculations, a y^+ of 11.63 sets the lower limit for the distance of the first cell, to the wall boundary, with the optimum position lying somewhere between 30 and 500, as suggested by Versteeg & Malalasekera [17]. It must also be remembered that whilst the first cell spacing is critical in accurate near wall flow modelling, enough cells should be placed within the boundary layer to resolve all the flow gradients. The use of wall functions therefore poses a special grid independence problem for near wall flows.

5.2 Near Wall Grid Independence Study

In this CFD flat plate investigation, a full independence study was carried out to determine the optimum boundary layer cell distribution. The study was carried out on the largest plate tested by Froude, the case of maximum turbulent flow. The wall roughness considered as being hydraulically smooth. It is known from the previous work done by Reynolds et al [6] that the transition from laminar flow to turbulent flow over a flat plate happens at a critical Reynolds number of $\approx 5\times10^6$. From Table 4.0 it is evident that for all but the shortest of plates and slowest of speeds that all of Froude's tests were conducted within the turbulent flow region. With the knowledge that the flow across Froude's plates was predominantly turbulent, it was necessary to select a turbulence model within CFX capable of modelling high Reynolds number flows. Within CFX there are two high Reynolds number turbulence models, the standard K-ε model and RNG K-ε model, both of which were tested.

Plate Length ft , (m)	Max Velocity (m/s)	Min Velocity (m/s)	Max Reynolds No.	Min Reynolds No.
50 (15.24)	5.08	0.25	68.0×10^6	3.3×10^6
1 (0.305)	5.08	0.25	1.4×10^6	66.9×10^3

Table 4.0 Reynolds Numbers For Froudes Plates

It was necessary in this independence study to consider both the maximum and minimum velocities at which the model was to be tested, since y^+ is function of velocity as well as cell spacing. Having to produce a grid suitable for operation over a range of Reynolds numbers caused a significant problem with regard to fixing the first cell size. This cell size was carefully selected to ensure that the y^+ remained within the 30 to 500 range for all Reynolds numbers. As well as a study into first cell spacing, a study was carried out to ensure that the solution to the flow problem was independent of the number cells in the Y-Direction.

Within CFX the grid propagation options allow either a uniform distribution or geometric progression along block edges. In this boundary layer grid independence study the geometric progression distribution was used in the Y-Direction and a simple uniform distribution in the X-Direction. The form of the geometric progression used by CFX can be found in Appendix 12. Within CFX the geometric propagation is controlled by the number of cells and a common factor. However, this is not really an effective way of controlling the cell distributions since it is not controlled by physical cell size. As it can be seen in Appendix 12 the cell distribution parameters in the geometric progression can be derived using the first and last cell sizes on a block edge, following the manipulation of the original formula. Using the first and last cell sizes to control the distribution in the Y-Direction, a detailed study was carried out to determine the optimum near wall cell spacing and its effect on skin friction estimation. The uniform distribution in the X-Direction consisted of 40 cells in the 2L upstream and downstream directions and 20 Cells along the plate itself. An example of Grid used in this study can be seen in Figure 5.0.

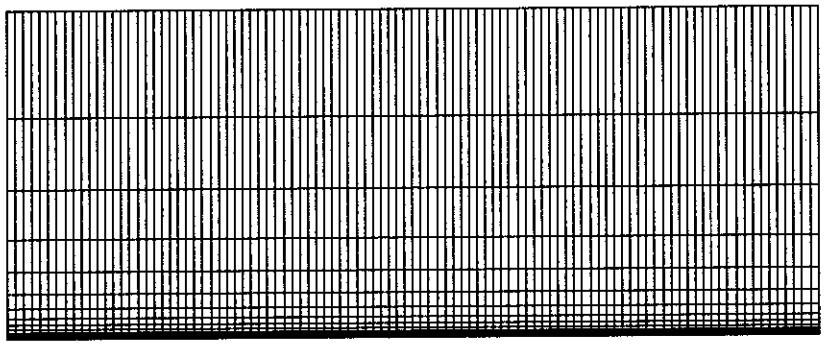

Figure 5.0 Example of Grid Used in Near Wall Grid Study

The outer cell in the Y-Direction had a fixed cell spacing of 10m and the near wall cell size was varied. In order to get an estimate of the cell size needed to give the correct y^+ for the high and low Reynolds numbers the following equation was used, from Flat Plate Boundary Layer Theory [19].

$$y^+ = 0.172 \cdot \left(\frac{\Delta y_P}{L} \right) \cdot \mathrm{Re}^{0.9} \qquad (5.5)$$

Using a $y^+ = 30$ as the criterion for the first cell size, the corresponding Δy_P was found for both the high and low Reynolds number flow conditions.

Velocity (m/s)	Reynolds No.	Estimate of y^+	First Cell Size Δy_P (m)
5.08	68.0×10^6	30	0.00024
0.254	3.3×10^6	30	0.00350

Table 5.0 Cell Sizes for 15.24m Flat Plate at High & Low Reynolds Numbers

As it can be seen from Table 5.0 the first cells sizes at the maximum and minimum Reynolds numbers vary quite dramatically when y^+ is fixed at 30. In fact the cell size for the high Reynolds number case is approximately 15 times smaller than that of the low Reynolds number case. Hence, if the same grid is to be used in solving both the high and low Reynolds number flow cases, the smallest first cell size should no smaller than 0.0035m in the Y-Direction if y^+ is to be kept above the lower limit of 30. Based on these estimates it was decided that the first cell size spacing would be set at 0.005m. Two CFX runs were subsequently carried out at the maximum and minimum Reynolds

numbers to check that the actual CFX calculated y^+ values fell within the bounds required. The results from the two CFX runs can be seen in Table 6.0. For the high Reynolds number case, the y^+ values lie with the range $30 \le y^+ \le 500$ using a cell spacing of 0.005m. However, for the low Reynolds number case, the y^+ values fall below these bounds, but above the absolute minimum value of 11.63. Based on the results from this study it was decided to stick with the first cell size of 0.005m since it seems to make good use of wall functions across the range of Reynolds numbers intended to be studied.

Velocity (m/s)	Reynolds No.	First Cell Size Δy_P	y^+ Along Plate Length
5.08	68.0×10^6	0.005	246-335
0.254	3.3×10^6	0.005	16-22

Table 6.0 CFX Calculated y^+ Values for a 15.24m Flat Plate

A brief study was subsequently carried out to determine the effect of the choice of y^+ on the actual calculated skin friction within the range of $30 \le y^+ \le 500$ for the 15.24m plate operating at the highest Reynolds number. The results in Table 7.0 show the results from five different CFX runs, each with a near wall cell size half that of the previous and outer cell size of 5.0m.

First Cell Size Δy_P	y^+ Along Plate Length	C_F (x 10^{-3})	No. Iterations	CPU Time (Sec)	Total No. Cells
0.005	246-335	2.37	649	8.56×10^2	4000
0.0025	126-171	2.36	1234	1.85×10^3	4300
0.00125	58-79	2.35	2981	4.83×10^3	4700
0.000625	30-40	2.36	5728	1.02×10^4	5100
0.000313	15-20	2.39	10452	1.96×10^5	5500

Table 7.0 Effect of Near Wall Cell Size on Skin Friction & Solution Time

It can be seen from these results that there is very little variation in drag coefficient with near wall cell size. However, it is obvious from Table 7.0 that the use of a small near cell size and hence small y^+ causes excessive computational effort to be used in formulating a solution with no added increase in accuracy. Although the reduction in the near wall cell size slightly increases the total number of cells within the

problem, this alone does not account for the 228 fold increase in CPU time needed to solve a problem, with an extra 1500 cells, with regard to the maximum and minimum near wall cell size cases.

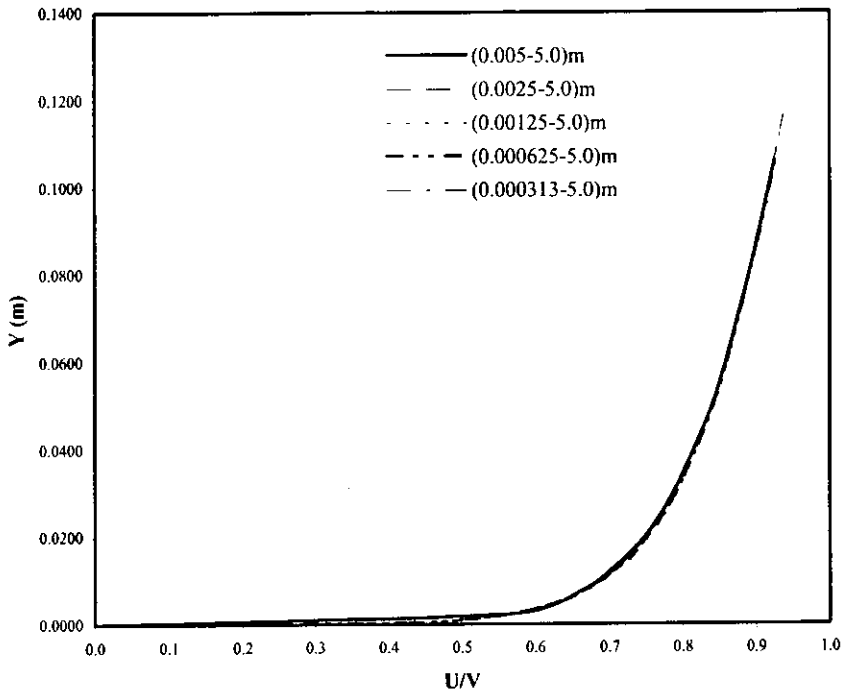

Figure 6.0 Boundary Layer Profile at X/L=1.0 For 15.24m Flat Plate

It should be noted that if the cell size is such that the y^+ falls below 5, and hence is within the purely laminar flow region, convergence is hard to achieve. This study therefore indicates the importance of selecting the correct near wall cell size in order to make good use of the wall functions provided, thereby conserving valuable computational resources.

Using the data generated by CFX for the above five conditions, a plot of the near wall boundary layer profile was produced at the trailing edge to show graphically the effect of using this wall function approach. As can be seen in Figure 6.0 the boundary layer profiles were identical for all the near cell wall spacing cases tested, as expected from wall function theory.

5.3 Outer Wall flow Support Grid Independence Study

Following the correct selection of the near wall grid spacing, a convergence study was carried out to determine the optimum outer grid cell size needed to provide the required distribution for flow support in the Y-Direction. The near wall grid spacing was fixed at 0.005m and the outer grid cell was varied between 10m and 1.25m until convergence was achieved. The distributions in the X-Direction were the same as those used in the near wall grid study and the flow speed was fixed at 5.08m/s.

Last Cell Size (m)	C_F (x 10^{-3})	No. Iterations	CPU Time (Sec)	Total No. Cells
10	2.390	293	1.68×10^{2}	2000
5	2.369	649	8.56×10^{2}	4000
2.5	2.365	1100	2.91×10^{3}	7400
1.25	2.364	1541	1.06×10^{4}	13300

Table 8.0 Outer Cell Independence Study

From Table 1.0 and Figure 7.0 it can be seen that full convergence on skin friction coefficient was reached when the outer cell size was fixed at 1.25m.

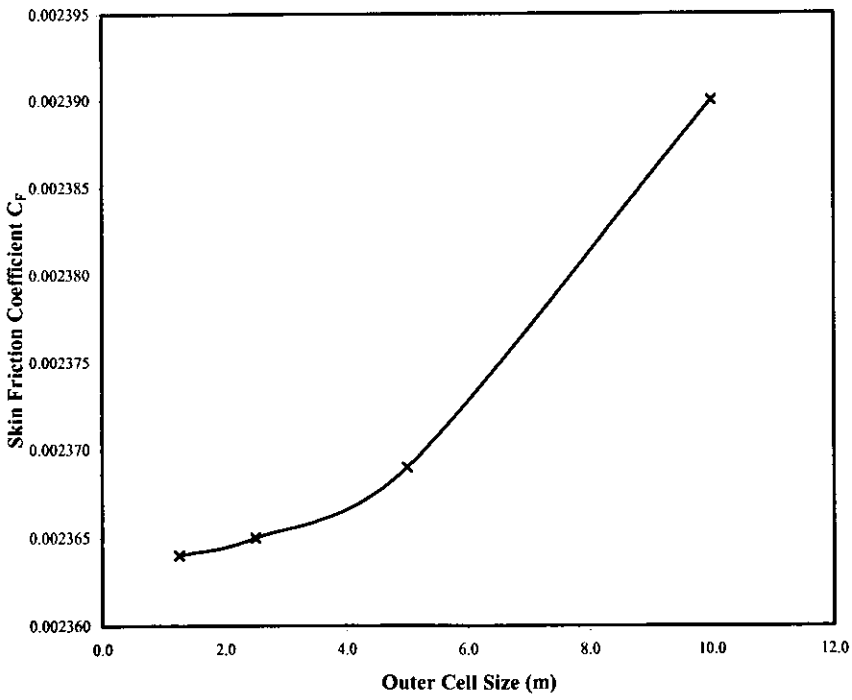

Figure 7.0 C_F Vs Outer Cell Size For 15.24m Flat Plate

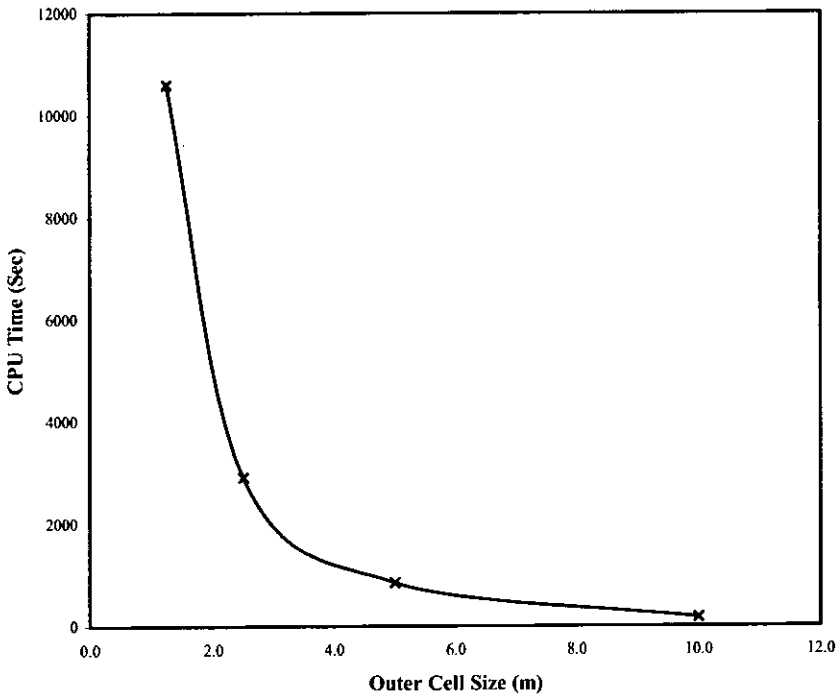

Figure 8.0 CPU Time Vs Outer Cell Size For 15.24m Flat Plate

It can be seen from Table 8.0 and Figure 8.0 that the number of Iterations and CPU Time sharply increase with decreasing outer cell size as a result of the increased Total No. of cells. Based on this data it was decided that the outer cell size of 2.5m would used in subsequent calculations since the small increased accuracy of the 1.25m case did not warrant the extra number of cells and hence increased CPU time.

5.4 Longitudinal Grid Independence Study

An independence study was carried out for the grid distribution along the length of the plate itself. Again the study was carried out on the 50ft (15.24m) plate at 5.08m/s. The grid propagation in the Y-Direction was set in accordance with the grid independent solution found in the boundary layer study i.e. 0.005m-2.5m. The propagation used on the upstream and down stream blocks 1 & 3 were set as geometric progressions, with outer cell sizes starting at 2.5m decreasing in size to 0.1m at the leading edge of the plate. The distribution used on the plate itself was a symmetric geometric progression. With a matched cell size of 0.1m at the leading edges and variable middle cell size. An example of the grid used in this can be seen in Figure 9.0; note the cell clustering at the leading and trailing edges of the plate.

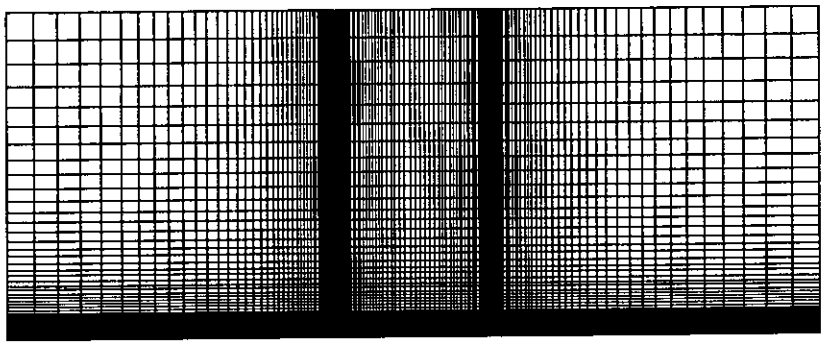

Figure 9.0 Example of Grid Used in Longitudinal Grid Independence Study

Middle Cell Size (m)	C_F (x 10^{-3})	No. Iterations	CPU Time (Sec)	Total No. Cells
4	2.380	1345	2.25×10^3	5464
2	2.374	1208	3.55×10^3	7548
1	2.373	1185	4.13×10^3	8732
0.5	2.372	1109	4.81×10^3	10434
0.25	2.372	1008	5.74×10^3	12728
0.125	2.372	906	6.69×10^3	15964

Table 9.0 Longitudinal Grid Independence Study Results

From Table 9.0 it can be seen that convergence on skin friction coefficient is achieved when the middle cell size of the geometric progression reaches a cell size of 0.5m. From the table, it can be seen that further reduction in middle cell size along the plate does not effect the skin friction coefficient. Hence, it can be said that the solution to this problem is grid independent.

The grids used subsequently in this investigation were hence based on the results found in this grid independence study. The X-Direction geometric progression distributions on the blocks for the different plate lengths tested were set with the same parameters as those derived for the 50ft (15.24m) plate tested in the independence study. However, the Y-Direction geometric progressions down on to the plate itself were slightly modified to ensure that the first cell size gave the correct y^+ value for the particular plate length.

6. Comparison of CFD Results with Experimental Data

Following the grid independence study and the determination of the optimum grid parameters necessary for accurately modelling a flat plate, the evaluation study into the

accuracy of viscous flow RANS modelling could be conducted. The aim of this investigation was to determine the best turbulence model for viscous accurate skin friction prediction and the associated effects of Reynolds number. The investigation involved further modelling Froudes plates of 50ft (15.24m), 16ft (4.88m), 1ft (0.30m) and a two ship scale high Reynolds number test cases of 500ft (152.40m) & 1000ft (304.8m). All of the results obtained where validated against Froudes original test data and the ITTC 1957 and Schoenherr correlation lines. All the raw data from the study can be found in the Appendix.

6.1 Differencing Scheme Effects on Accuracy

In Chapter 5. the problems associated with grid quality were investigated. However, obtaining an accurate flow solution for a particular grid has as much to do with the choice of differencing scheme employed as the number of cells used to discretize the problem. The choice of differencing scheme dictates the way in which the partial derivatives in the governing Navier-Stokes equations are replaced with algebraic difference quotients based on the flow field variables at the faces of the control volumes. There are a variety differencing schemes used in CFD, all with varying orders of accuracy. The use of a greater number of surrounding control volume faces in formulating the difference quotients usually constitutes a higher order accurate differencing scheme. As with grid independence, the choice of the differencing scheme used for a particular flow solution depends on the flow type and the degree of accuracy expected from the flow solution. High order accurate differencing schemes often have the advantage over the lower order schemes that they generally need fewer total grid points to obtain comparable overall accuracy, at the expense of increased computer time. However, lower order schemes are often more robust than higher order schemes and can cause less convergence problems.

In this investigation, three of the most common differencing schemes employed in CFD were investigated. UPWIND (First Order), QUICK (Third Order) and HYBRID (Second Order). The UPWIND differencing scheme forms the difference quotients based on the value of the upstream control volume face, whereas the QUICK (Quadratic Upstream Interpolation for Convective Kinetics) used a three point upstream weighted quadratic interpolation. The HYBRID interpolation combines an UPWIND interpolation with that a CENTRAL differencing scheme, which uses one upstream and one

downstream face for interpolation. All the tests were carried out on the 15.24m plate using the standard K-ε model.

Flow Field Variable	First Order	Third Order
U	UPWIND	QUICK
V	UPWIND	QUICK
P	UPWIND	QUICK
K	UPWIND	HYBRID
ε	UPWIND	HYBRID

Table 10.0 Differencing Schemes Tested

Table 10.0 above shows the differencing schemes tested on the 15.24m plate. For the high order study, the QUICK differencing scheme was unable to be implemented on the turbulence equations K & ε, since this gave rise to non-convergent flow solutions resulting from negative values of K & ε. The HYBRID scheme was thus used instead, ensuring that K & ε remained positive. Although the HYBRID scheme is second order, the overall accuracy of the flow solution is largely unaffected, since K & ε are dominated by production and dissipation. The results from the study can be seen in Figure 10.0.

As it can be seen from Figure 10.0 there is only a slight increase in accuracy when the third order differencing scheme is used for solving the flow over the 15.24m plate. It was however noted, that the use of the QUICK scheme resulted in an increased solution time compared with that of the UPWIND solution. Depending on flow velocity, this increase varied between 15-45%. With hindsight, this is not at all surprising, since the grid used in this study was refined with extreme accuracy using the QUICK differencing scheme. The use of the QUICK differencing schemes throughout the boundary positioning and independence study's was done to ensure a high degree of accuracy in the final comparison studies. If the grid had been refined using the UPWIND differencing scheme, it is envisaged that there would be a noticeable increase in accuracy if a higher order scheme was subsequently used. Following this route would however have resulted in a further independence study, to confirm that the maximum level of accuracy had been achieved and not just an increase in accuracy from the UPWIND solution.

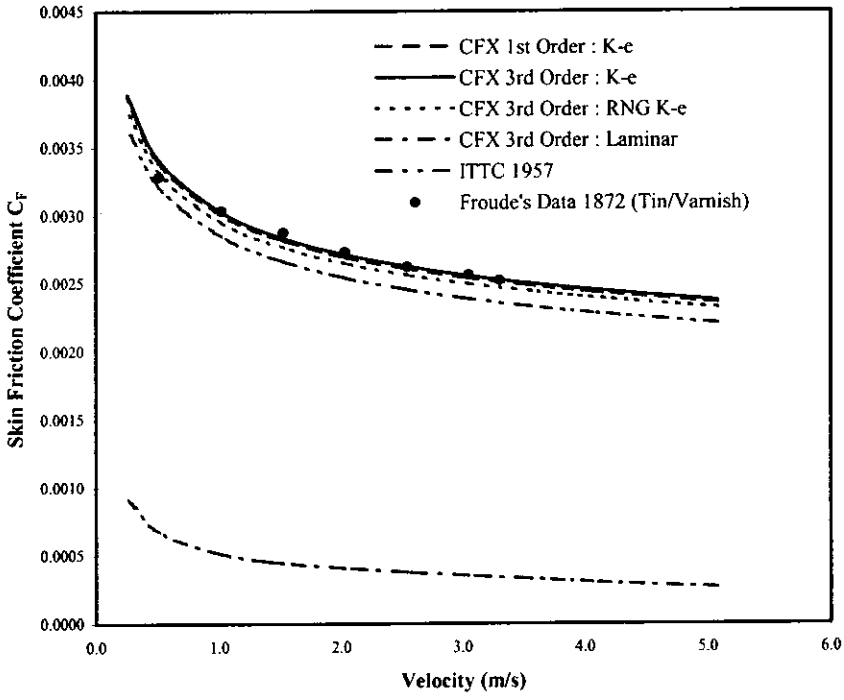

Figure 10.0 C_F Vs Velocity for a 15.24m Plate

6.2 Comparison of High Reynolds Number Turbulence Models

A study was carried out to determine which out of the two high Reynolds number turbulence models available within CFX gave the most accurate viscous drag predictions. The standard *K*-ε and the RNG *K*-ε turbulence models were verified for the highest and lowest Reynolds numbers plate experiments tested by Froude (i.e. the 1ft (0.305m) & 50ft (15.24m) plate cases). The results were assessed using Froudes experimental data as a benchmark. The results from the study can be seen in Figure 10.0 & Figure 11.0. From Figure 10.0 it obvious that there is little difference in the accuracy of the two turbulence models when validated against the results from Froudes experimental data. Although not obvious from the plot, the standard *K*-ε turbulence model is in fact 2% more accurate in predicting the skin friction than the RNG *K*-ε model, providing a skin friction estimate within 99.7% of Froudes actual experimental value. However, the results from the low Reynolds number study on the 1ft (0.305m) plate do not show good agreement with Froudes experimental data as indicated in Figure 11.0. The skin friction estimates calculated using the two different turbulence models

show good agreement with each other as for the high Reynolds number case. However, they both seem to over predict the viscous drag by 15-50%, depending on surface finish of the plates the data is validated against. It is believed that the source of this error is due to the turbulence model's inability of simulating transition from laminar to turbulent flow. The problems associated with transition will be discussed in more detail in Chapter 6.3.

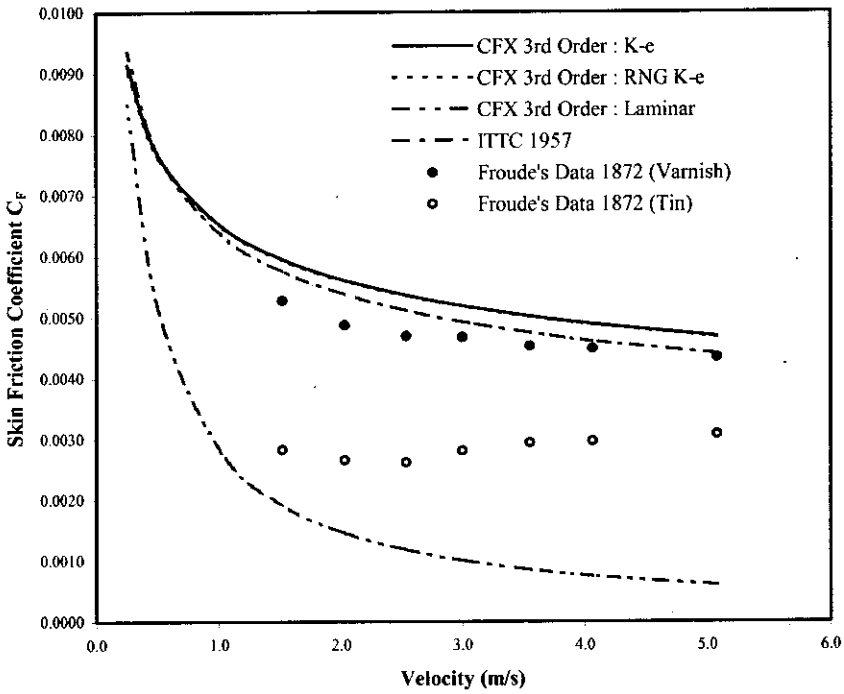

Figure 11.0 C_F Vs Velocity for a 0.305m Plate

Based on the results found in this study, the standard K-ε model was considered the most accurate turbulence model for solving viscous flow problems, and hence was used for all the subsequent studies presented in this report.

6.3 Laminar-Turbulent Transition Problem

In Chapter 2.2 the phenomena of laminar-turbulent transition was discussed, and it is believed that this is responsible for the error in the skin friction prediction at low Reynolds numbers, as identified in Chapter 6.2. Looking at the experimental data plotted in Figure 11.0 and considering the Reynolds number range over which the data corresponds (4.0×10^5 – 1.0×10^6), it is obvious that the flow is within the typical laminar-turbulent transition region of 3.0×10^5 – 1.0×10^7. The effect of surface

roughness on skin friction is also highlighted in Figure 11.0 on comparison of the experimental data for the varnished and tin foil coated plates tested by Froude. The rougher varnished plate has the effect of tripping the initial laminar boundary layer into becoming turbulent closer to the leading edge, resulting in a greater experienced total viscous drag force. However, the smooth tin foil covered plate has a greater region of laminar flow extending further aft along its surface which is triggered into turbulent flow much later, which results in greatly reduced skin friction.

The discrepancy between Froude's experimental data and the theoretical results obtained using CFX are as a result of the flow codes lack of simulation of this laminar-turbulent transition region. When solving fluid flows using CFX the problem has to be specified as being either laminar or turbulent. Hence, laminar or turbulent flow is simulated over the whole length of the plate from the leading edge, which is physically incorrect. However, the assumption that the flow is fully turbulent over the whole length of the plate is valid for plates travelling at high Reynolds numbers greater than 5.0×10^6. At these high Reynolds numbers, the contribution to skin friction resulting from the laminar boundary layer tends to zero, since transition happens almost instantaneously at the leading edge. Hence, there is good agreement between the experimental and theoretical results, as shown in Figure 10.0.

At low Reynolds numbers below 5.0×10^6 the situation is reversed and the laminar boundary layer contribution to viscous drag becomes significant and the assumption that the flow is fully turbulent does not hold. This therefore results in an overestimate of the viscous drag, as shown in Figure 11.0. With regard to CFX, there is no simple solution to the problem of transitional flow since the problem must be specified as either laminar or turbulent. The only way to model this problem, taking into account the laminar and turbulent flow region effects, would be to model each region separately. An estimate could be made of the length of surface in which the flow remains laminar, and the flow over its surface solved accordingly. The outlet boundary condition from this solution could then be applied as the inlet boundary condition for the remainder of the plate and solved using the turbulent flow condition. The total skin friction could then be calculated from the sum of the forces from the two solutions.

Other CFD studies such as those carried out by Chung & Min [20] have simulated laminar-turbulent transition using a triggering method in which the critical local Reynolds number or location of transition is specified on the body. However, for

most practical full-scale ship flow calculations the problems associated with transition can be ignored, since the flow is predominately turbulent over the whole body. Therefore, only at very small model scales should the problem of flow transition be addressed.

6.4 Comparison of CFD Results with Skin Friction Lines

A study was conducted to asses the overall performance of the standard K-ε turbulence model over a range of Reynolds numbers from model to full scale, similar to that conducted by Dolphin [21] on the Baldwin-Lomax turbulence model. The results obtained were compared with the empirical skin friction correlation lines of Schoenherr and the ITTC. In order to make valid comparisons, further CFX runs were carried out to provide skin friction data at intermediate and high Reynolds numbers. The runs were carried out on flat plates of 16ft (4.877m), 500ft (152.4m) & 1000ft (304.8m). The resistance curves for these plates are shown in Figure 12.0, Figure 13.0 & Figure 14.0.

All of the skin friction data obtained for standard K-ε turbulence model and laminar studies to third order were subsequently plotted on a Schoenherr Log-Log graph, along with the empirical skin friction lines of Schoenherr and the ITTC and Froude's data as shown in Figure 15.0. When the CFD data is compared with the ITTC model-ship correlation line the following trends were identified.

- Between Reynolds numbers 5.0×10^4 and 1.0×10^6, there is good agreement between the CFD data and ITTC line, probably due to the modified slope of the ITTC line.
- Between Reynolds numbers 1.0×10^6 and 1.0×10^9, there seems to be a constant over prediction in skin friction by the CFD.

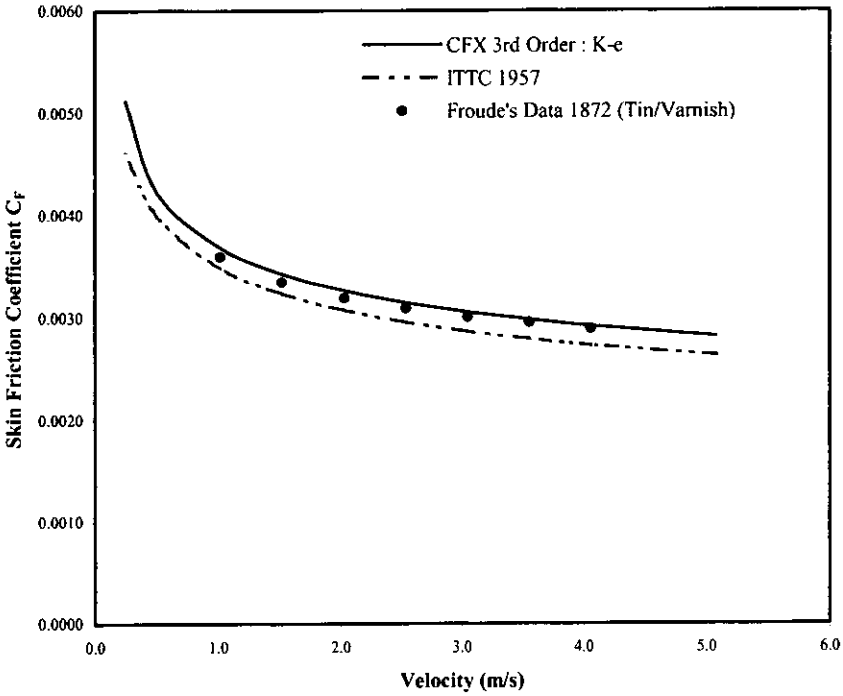

Figure 12.0 C_F Vs Velocity for a 4.877m Plate

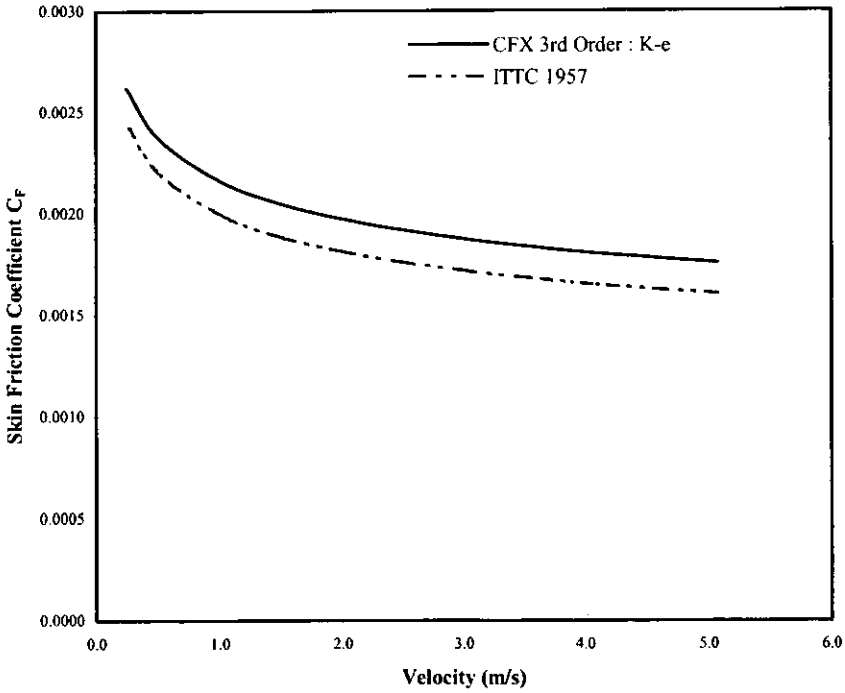

Figure 13.0 C_F Vs Velocity for a 152.4m Plate

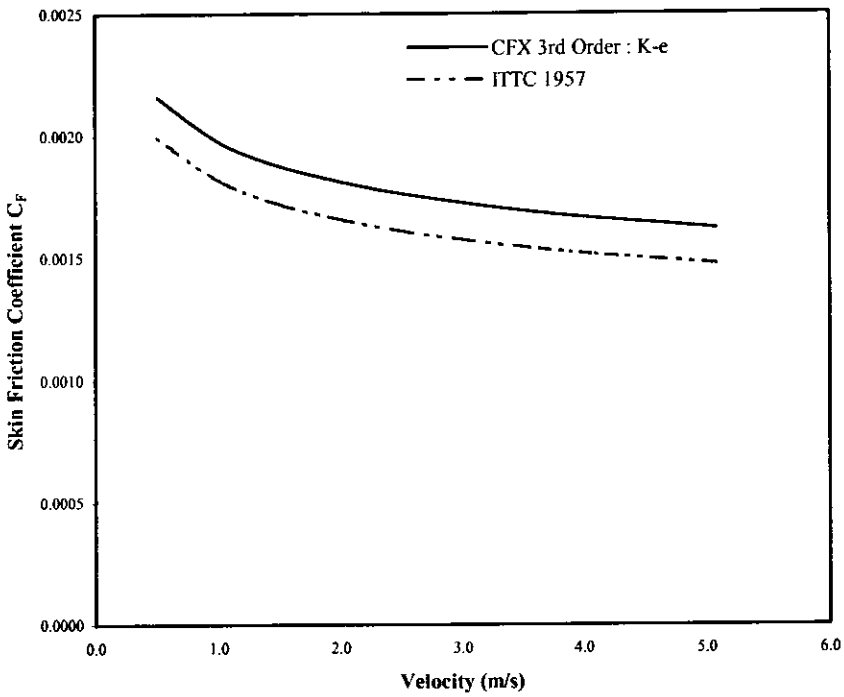

Figure 14.0 C_F Vs Velocity for a 304.8m Plate

The following trends were identified on comparing the CFD data with Schoenherr's line.

- There is general linear agreement between the CFD data and the Schoenherr line across the whole range of Reynolds numbers.
- Between Reynolds numbers 1.0×10^5 and 2.0×10^7, there is a constant under estimate in skin friction by the CFD, probably due to the inclusion of aspect ratio and edge effects in Schoenherr's original data.
- Between Reynolds numbers 2.0×10^7 and 1.0×10^9, there is a constant over prediction in the skin friction by the CFD.

From this study it can therefore be concluded that standard K-ε turbulence model generally performs well over the range of Reynolds numbers investigated, with only slight differences compared to empirical friction lines of the Schoenherr and the ITTC. However, as highlighted by Kodama [22], only after conducting full scale measured wake surveys can a turbulence model be considered as being fully validated. Since, a

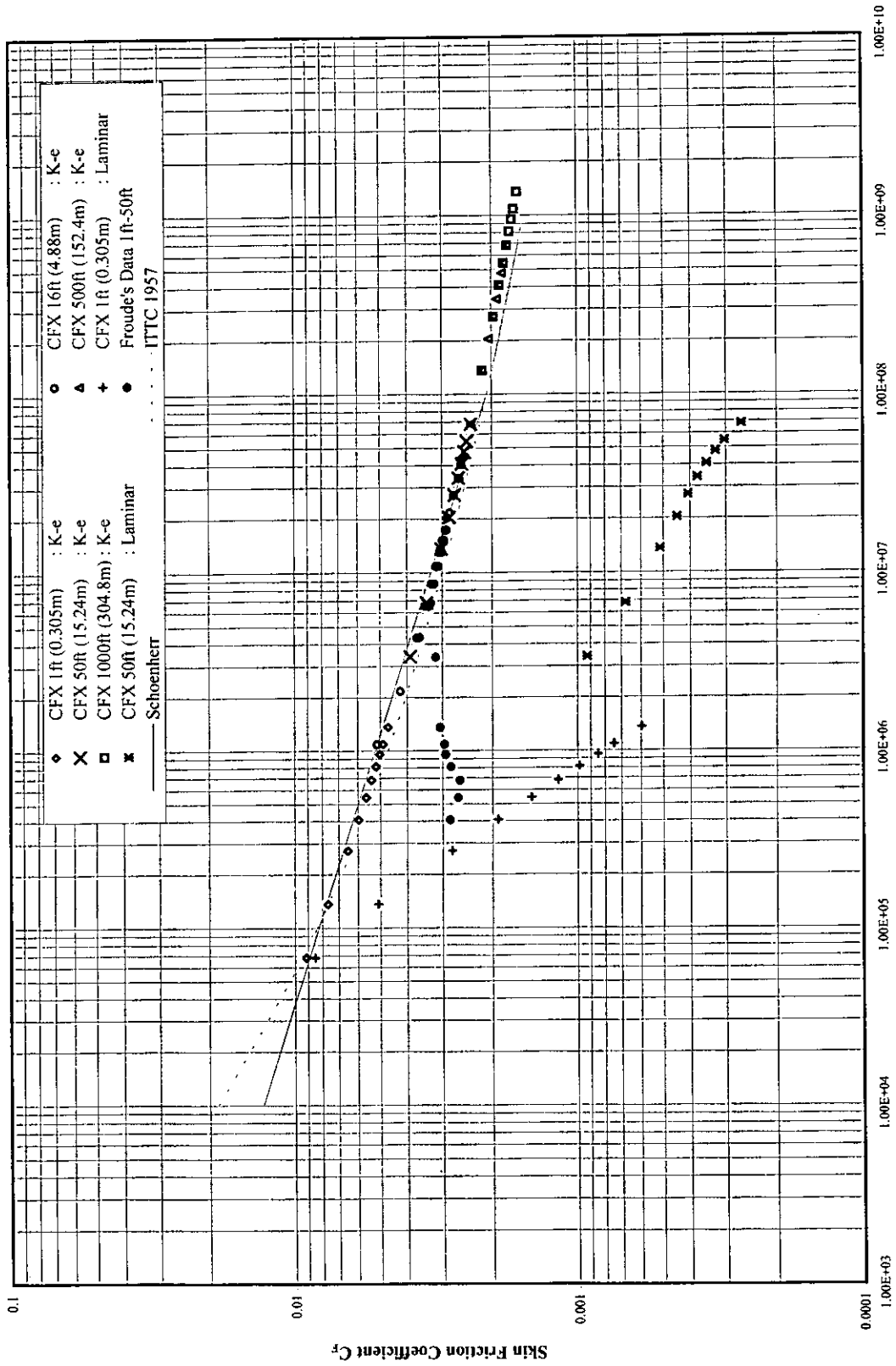

Figure 15.0 Schoenherr's Log-Log Graph for Friction Formulation

good turbulence model should be able to capture the Reynolds number dependence of the wake from model to full scale.

6.5 Numerically Derived Form of Resistance Correlation Line

Based on all the experimental skin friction data obtained for the standard K-ε turbulence model, a CFD modified Schoenherr skin friction formula was derived using the Prandtl Logarithmic approach discussed in Chapter 2.2. A linear least squares regression fit was then carried out on all of the results to obtain the coefficients A & B in Equation (2.5). The regression plot of the data can be seen in Figure 16.0. The modified Schoenherr formula based on the regression analysis of the CFD data is given by Equation (6.1).

$$\frac{1}{\sqrt{C_F}} = 4.06\log_{10}(\mathrm{Re}\cdot C_F) - 0.725 \qquad (6.1)$$

As it can be seen, the form of Equation (6.1) nearly identical to the one derived by Schoenherr from experimental data, with identical gradient and slight offset.

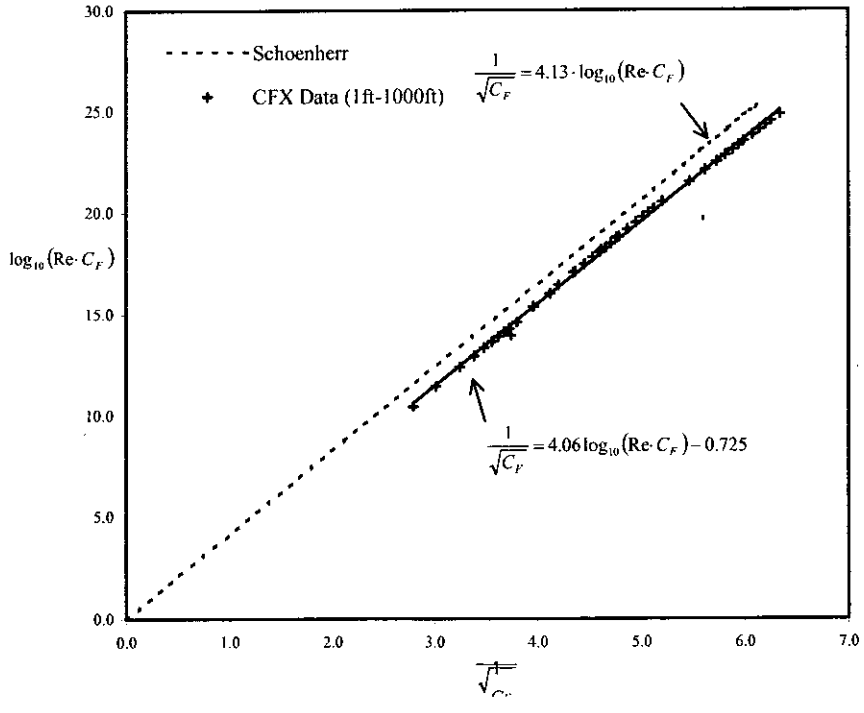

Figure 16.0 Evaluation of New Prandtl Logarithmic Skin Friction formula

6.6 Simulating Wall roughness

A brief investigation was carried out to determine how the effect of plate roughness could be simulated, since in all the calculations thus far, the plates were assumed as being hydraulically smooth. The study was carried out on the 50ft (15.24m) plate. As mentioned in Chapter 5.1, when using wall functions the effect of wall roughness can be simulated by decreasing the Log-Layer constant E. The skin friction results for smooth wall condition where $E = 9.793$ were compared with two rough wall cases; where $E = 4.897$ and $E = 2.449$. The results are plotted in Figure 17.0. As can be seen, decreasing the value of the Log-Layer results in an increase in predicted skin friction. Using a Log-Layer constant half that of smooth wall value (9.793) results in a 11% increase in the predicted viscous drag, and the use of a value a quarter of the smooth wall value results in a 22% increase in viscous drag. A linear relationship between Log-Layer constant and skin friction appears to have been identified.

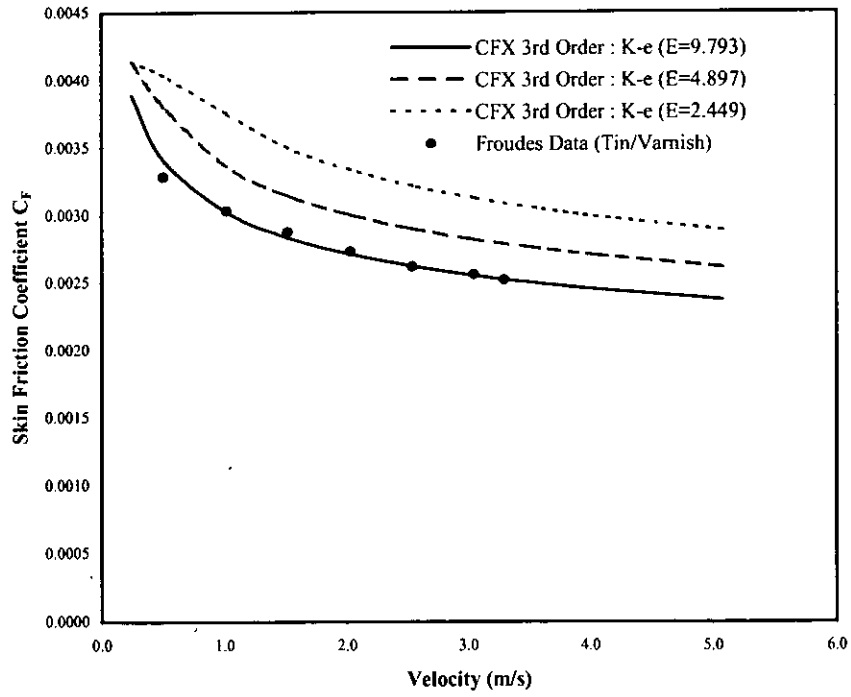

Figure 17.0 Variation of Skin Friction With Log Layer Constant for a 15.24m Plate

It is however possible to select values of the Log-Layer constant based on experimental data on sand roughness, values of which can be found in Schlichting [19]. However,

finding the sand roughness and its corresponding Log-Layer constant for a particular surface is very difficult. The only accurate way of determining the Log-Layer constant for a particular surface finish, say a painted ship hull, would be to conduct a flat plate experiment. The Log-Layer constant in the CFD calculations could then be adjusted to make the calculated skin friction consistent with those found in the experiment.

7. Conclusions

A flat plate geometry was used to determine the optimum model and grid conditions necessary for accurate skin friction estimation, when using a RANS code for flow solution. This investigation has highlighted the complex procedures that have to be carried out on even the simplest of viscous flow problems, in order to obtain accurate viscous skin friction estimates. However, the procedures carried out in this study apply equally to the modelling of any viscous flow problem, be it a simple pipe flow or the flow round complex ship geometry. The only difference between the ship flow problem and the flow about a flat plate, is that the model and grid considerations are further complicated by the existence of viscous pressure forces. The important CFD procedures that must be carried out in any high quality viscous CFD study are listed below.

- Correct Boundary Condition Selection
- Correct Boundary Positioning Study
- Optimum Near Wall Grid Spacing Study
- A full Grid Independence Study
- Differencing Scheme Solution Accuracy Study
- Correct Turbulence Model Selection

The following general conclusions were draw from this skin friction investigation, based on the headings above.

1) Correct model boundary condition selection and positioning are essential in forming a well-posed problem capable of efficient solution using a RANS code solver.

2) Detailed near wall and whole fluid domain independence studies are necessary if CFD solutions are to be regarded as being grid independent and of the highest level of accuracy.
3) Effects of Reynolds number on the near wall grid spacing must be taken into account when dealing with a flow problems operating over a range of velocities.
4) Initial specification of the level of accuracy expected from the results is essential, in order to make efficient use of computational resources.

The following main conclusions were drawn from the comparisons made between the CFD results and those of Froude and the empirical skin friction lines.

1) The standard K-ε and RNG K-ε turbulence models both performed well over a range of Reynolds numbers, with the standard K-ε model providing a 2% more accurate correlation with Froude's data than the RNG K-ε turbulence model at high Reynolds numbers.
2) With regard to the skin friction estimation at low Reynolds number, the CFD results were in error due to the RANS code's inability in simulating laminar-turbulent transition.
3) There is general correlation between the CFD results and the correlation lines of the ITTC and Schoenherr over the range of Reynolds numbers investigated, with specific differences within certain bounds of Reynolds number.
4) A modified Schoenherr formula was derived from all the CFD data, providing a formula not dissimilar to that derived by Schoenherr himself from the regression analysis of experimental data.
5) It was shown that surface roughness could be simulated by suitably modifying the Log-Layer constant within the turbulence model wall function.

Acknowledgements

The research described in this report was part of an industrial research contract into Maritime CFD funded by Hamworthy Marine Technology, Poole, Dorset, U.K.

References

[1] Froude, W. (1872). "Experiments on Surface-friction experienced by a Plane moving through water", 42nd Report by the British Association for the Advancement of Science.

[2] Froude, W. (1874). "Report to the lords Commissioners of the Admiralty on Experiments for the Determination of the Frictional Resistance of Water on a surface, under various conditions, performed at Chelston Cross, under the Authority of their Lordships", 44th Report by the British Association for the Advancement of Science.

[3] Society of Naval Architects and Marine Engineers (1988). "Principles of Naval Architecture", Volume II, Resistance, Propulsion and vibration.

[4] Payne, M.P. (1936). "Historical note on the Derivation of Froude's Skin Friction Constants", Trans. INA. Vol.78.

[5] Froude, W. (1874). "On Experiments with HMS Greyhound", Trans INA. Vol.15.

[6] Reynolds, O. (1883). "An Experimental Investigation of the Circumstances which Determine whether the Motion of Water shall be Direct or Sinuous, and of the Law of Resistance in Parallel Channels", Phil. Trans. Roy. Soc. 174.

[7] Blasius, H. (1908). "Grenzschichichichten in Flussigkeiten mit kleiner Reibung", Z. Math. Phys. 56.

[8] Prandtl, L. (1921). "Ergebnisse der Aerodynamischen Versuchsanstalt zu Goettingen", Abhandlungen aus dem Aerodynamischen Institut, Aachen.

[9] Prandtl, L. (1927,32). "Ergebnisse der Aerodynamischen Versuchsanstalt zu Goettingen", III Lieferung (1927), IV Lieferung (1932).

[10]Schoenherr, K.E. (1932). "Resistance of flat Surfaces Moving Through a Fluid", Trans. Soc. Nav. Arch. and Mar. Eng. 40.

[11] ITTC (1957). "Proceedings of the 8th ITTC", Madrid, Spain.

[12] Bertram, V. (1993). "Economical Aspects of CFD", 19th WEGEMT School, Nantes.

[13] Martinelli, L. (1993). "CFD Applications in Ship Design", 19th WEGEMT School, Nantes.

[14] Marzi, J. & Y.E.D. (1994). "On the Integration of CFD in Ship Design", ICCAS, Bremen.

[15] ITTC (1996). "Proceedings of the 21st ITTC", Volume I, Trondheim, Norway.

[16] Anderson, J.D. (1995). "Computational Fluid Dynamics, The Basics with Applications", McGraw-Hill International Editions, Mechanical Engineering Series.

[17] Versteeg, H.K. & Malalasekera, W. (1995) "An introduction to Computational Fluid Dynamics", Longman Scientific & Technical.

[18] CFX International (1996). "CFX 4.2 User Guide" CFX International, Harwell Laboratories, Oxfordshire, OX11 0RA, U.K.

[19] Schlichting, H. (1966). "Boundary Layer Theory", McGraw-Hill, New York.

[20] Chung, K.N. & Min, K.S. (1998) "A Study of Viscous Flow Field Around an Axisymmetric Body with Propeller", Proceedings of the Third Osaka Colloquium on Advanced CFD Applications to Ship flow and Hull Form Design, Osaka Prefecture University, Osaka.

[21] Dolphin, G. (1996). " Evaluation of CFD for Flat Plate Axisymmetric and Ship Geometries from Model to Full Scale Reynolds numbers", Master's Thesis, the University of Iowa, Iowa City, IA.

[22] Kodama, Y. (1998). "Scope of CFD for Computing Ship Flows", Proceedings of the Third Osaka Colloquium on Advanced CFD Applications to Ship flow and Hull Form Design, Osaka Prefecture University, Osaka.

Appendices

A. Command File For 50ft (15.24m) Plate Travelling at 5.08m/s

```
>>CFX4
  >>OPTIONS
    TWO DIMENSIONS
    BODY FITTED GRID
    CARTESIAN COORDINATES
    TURBULENT FLOW
    ISOTHERMAL FLOW
    INCOMPRESSIBLE FLOW
    STEADY STATE
>>MODEL DATA
  >>DIFFERENCING SCHEME
    U VELOCITY 'QUICK'
    V VELOCITY 'QUICK'
    K 'HYBRID'
    EPSILON 'HYBRID'
  >>SET INITIAL GUESS
    >>SET CONSTANT GUESS
      U VELOCITY 5.0800E+00
      V VELOCITY 0.0000E+00
      PRESSURE 0.0000E+00
      K 1.0000E-03
      EPSILON 1.0000E-03
  >>TITLE
    PROBLEM TITLE 'BOUNDARY CONDITION STUDY'
  >>PHYSICAL PROPERTIES
    >>STANDARD FLUID
      FLUID 'WATER'
      STANDARD FLUID REFERENCE TEMPERATURE 2.7300E+02
    >>TURBULENCE PARAMETERS
      >>TURBULENCE MODEL
        TURBULENCE MODEL 'K-EPSILON'
>>SOLVER DATA
  >>PROGRAM CONTROL
    MAXIMUM NUMBER OF ITERATIONS 2000
    MAXIMUM CPU TIME 14400
    OUTPUT MONITOR POSITION 1.524000E+01 7.620000E+00
    0.000000E+00
    MASS SOURCE TOLERANCE 1.0000E-06
  >>EQUATION SOLVERS
    U VELOCITY 'AMG'
    V VELOCITY 'AMG'
    PRESSURE 'AMG'
    K 'AMG'
    EPSILON 'AMG'
  >>PRESSURE CORRECTION
    PISO
  >>UNDER RELAXATION FACTORS
    U VELOCITY 7.5000E-01
```

```
    V VELOCITY 7.5000E-01
    PRESSURE 1.000E+00
    VISCOSITY 1.0000E+00
    K 7.5000E-01
    EPSILON 7.5000E-01
>>CREATE GRID
  >>INPUT GRID
    READ GRID FILE
    FORMATTED
>>MODEL BOUNDARY CONDITIONS
  >>MASS FLOW BOUNDARY CONDITIONS
    FLUXES 1* 1.000000E+00
    FRACTIONAL MASS FLOW SPECIFIED
  >>SET VARIABLES
    PATCH NAME 'FACE-NUMBER-7'
    U VELOCITY 5.0800E+00
    V VELOCITY 0.0000E+00
    PRESSURE 0.0000E+00
    K 1.0000E-03
    EPSILON 1.0000E-03
  >>SET VARIABLES
    PATCH NAME 'FACE-NUMBER-8'
    U VELOCITY 5.0800E+00
    V VELOCITY 0.0000E+00
    PRESSURE 0.0000E+00
  >>SET VARIABLES
    PATCH NAME 'FACE-NUMBER-11'
    U VELOCITY 5.0800E+00
    V VELOCITY 0.0000E+00
    PRESSURE 0.0000E+00
  >>SET VARIABLES
    PATCH NAME 'FACE-NUMBER-14'
    U VELOCITY 5.0800E+00
    V VELOCITY 0.0000E+00
    PRESSURE 0.0000E+00
  >>WALL BOUNDARY CONDITIONS
    PATCH NAME 'FACE-NUMBER-13'
>>OUTPUT OPTIONS
  >>PRINT OPTIONS
    >>WHAT
      WALL PRINTING
>>STOP
```

B. CFX Grid Geometric Propagation Formulae

$$D = \sum_{1}^{n} ar^{i-1} = a + ar + ar^2 + ar^3 + \ldots + ar^{n-1}$$

Where:

D	Block edge length (Sum of cell widths)
a	Last Cell width
ar^{n-1}	First cell width
n	Number of cells
r	Common ratio

Using the identity, $\sum_{1}^{n} ar^{i-1} = a\frac{(1-r^n)}{1-r}$ it can be shown that the common ratio can found using the formula below by specifying first and last cell size.

$$r = \frac{a - D}{ar^{n-1} - D}$$

Similarly, it can be shown that the number off cells needed to produce the geometric progression with the specified first and last cell sizes.

$$n = \frac{\log_{10}\left(D\frac{r-1}{a} + 1\right)}{\log_{10} r}$$

C. Data for 50ft (15.24m) Plate

Grid Information

Y-Distribution (Blocks 1,2 &3)	: 74 GP 1.09	(0.005m-2.5m)
X-Distribution (Blocks 1 & 3)	: 40 GP 0.92	(0.1m-2.5m)
X-Distribution (Block 2)	: 61 SYM GP 1.06	(0.1m-0.5m)
Total No. Cells	:10434	

Laminar Flow Results

Differencing: u & v (Quick)

Velocity	Reynolds No.	Skin Friction	C_F	No. It	CPU Time
5.08	6.80E+07	50.22	0.000265	130	4.13E+02
4.06	5.44E+07	36.84	0.000303	131	4.36E+02
3.56	4.76E+07	30.30	0.000326	132	4.15E+02
3.05	4.08E+07	23.94	0.000350	132	4.34E+02
2.54	3.40E+07	17.90	0.000377	120	4.47E+02
2.03	2.72E+07	12.36	0.000407	138	4.35E+02
1.52	2.04E+07	7.61	0.000445	192	5.83E+02
1.02	1.36E+07	3.89	0.000512	217	6.70E+02
0.51	6.80E+06	1.28	0.000676	213	6.58E+02
0.25	3.40E+06	0.44	0.000924	134	4.62E+02

Turbulent Flow Results

Turbulence Model: K-ε

Differencing: u & v (UPWIND), K & ε (UPWIND)

Log-Law Constant: 9.793

Velocity	Reynolds No.	Skin Friction	C_F	No. It	CPU Time
5.08	6.80E+07	447.40	0.002357	906	4.20E+03
4.06	5.44E+07	295.40	0.002432	907	4.05E+03
3.56	4.76E+07	230.60	0.002479	907	4.12E+03
3.05	4.08E+07	173.22	0.002535	904	4.10E+03
2.54	3.40E+07	123.56	0.002604	898	4.10E+03
2.03	2.72E+07	81.76	0.002692	886	4.08E+03
1.52	2.04E+07	48.08	0.002815	871	4.08E+03
1.02	1.36E+07	22.80	0.003003	801	3.65E+03
0.51	6.80E+06	6.42	0.003384	806	3.70E+03
0.25	3.40E+06	1.83	0.003864	877	3.96E+03

Turbulent Flow Results

Turbulence Model: K-ε

Differencing: u & v (QUICK), K & ε (HYBRID)

Log-Law Constant: 9.793

Velocity	Reynolds No.	Skin Friction	C_F	No. It	CPU Time
5.08	6.80E+07	450.20	0.002372	1109	4.81E+03
4.06	5.44E+07	297.40	0.002448	1078	5.09E+03
3.56	4.76E+07	232.00	0.002495	1045	5.03E+03
3.05	4.08E+07	174.38	0.002552	1023	4.94E+03
2.54	3.40E+07	124.40	0.002622	1007	4.57E+03
2.03	2.72E+07	82.32	0.002711	986	4.51E+03
1.52	2.04E+07	48.40	0.002833	929	4.29E+03
1.02	1.36E+07	22.96	0.003024	835	4.03E+03
0.51	6.80E+06	6.47	0.003407	752	3.31E+03
0.25	3.40E+06	1.85	0.003890	838	3.21E+03

Turbulent Flow Results

Turbulence Model: K-ε

Differencing: u & v (QUICK), K & ε (HYBRID)

Log-Law Constant: 4.897

Velocity	Reynolds No.	Skin Friction	C_F	No. It	CPU Time
5.08	6.80E+07	496.00	0.002613	1235	6.15E+03
4.06	5.44E+07	328.00	0.002700	1198	5.40E+03
3.56	4.76E+07	256.20	0.002755	1160	5.20E+03
3.05	4.08E+07	192.60	0.002819	1142	4.88E+03
2.54	3.40E+07	137.54	0.002899	1123	4.66E+03
2.03	2.72E+07	91.14	0.003001	1077	5.03E+03
1.52	2.04E+07	53.68	0.003142	1024	4.75E+03
1.02	1.36E+07	25.52	0.003361	936	4.16E+03
0.51	6.80E+06	7.22	0.003803	817	3.78E+03
0.25	3.40E+06	1.96	0.004132	874	4.09E+03

Turbulent Flow Results

Turbulence Model: K-ε

Differencing: u & v (QUICK), K & ε (HYBRID)

Log-Law Constant: 2.449

Velocity	Reynolds No.	Skin Friction	C_F	No. It	CPU Time
5.08	6.80E+07	548.20	0.002888	1370	6.48E+03
4.06	5.44E+07	363.00	0.002988	1310	6.63E+03
3.56	4.76E+07	283.80	0.003052	1270	6.37E+03
3.05	4.08E+07	213.60	0.003126	1244	6.75E+03
2.54	3.40E+07	152.68	0.003218	1219	5.85E+03
2.03	2.72E+07	101.30	0.003336	1178	5.73E+03
1.52	2.04E+07	59.78	0.003500	1129	5.56E+03
1.02	1.36E+07	28.50	0.003754	1033	5.16E+03
0.51	6.80E+06	7.652	0.004032	851	3.90E+03
0.25	3.40E+06	1.962	0.004135	874	4.17E+03

Turbulent Flow Results

Turbulence Model: K-ε RNG

Differencing: u & v (QUICK), K & ε (HYBRID)

Log-Law Constant: 9.793

Velocity	Reynolds No.	Skin Friction	C_F	No. It	CPU Time
5.08	6.80E+07	440.20	0.002319	915	4.01E+03
4.06	5.44E+07	290.60	0.002392	970	4.15E+03
3.56	4.76E+07	226.80	0.002439	978	4.13E+03
3.05	4.08E+07	170.36	0.002493	1006	4.26E+03
2.54	3.40E+07	121.48	0.002560	1024	4.50E+03
2.03	2.72E+07	80.36	0.002646	1090	4.60E+03
1.52	2.04E+07	47.22	0.002764	1126	5.15E+03
1.02	1.36E+07	22.38	0.002948	1130	5.13E+03
0.51	6.80E+06	6.30	0.003318	922	4.35E+03
0.25	3.40E+06	1.80	0.003787	942	4.48E+03

ITTC 1957 Model-Ship correlation Line

Velocity	Reynolds No.	Skin Friction	C_F
5.08	6.80E+07	418.51	0.002205
4.06	5.44E+07	276.41	0.002280
3.56	4.76E+07	216.90	0.002327
3.05	4.08E+07	163.04	0.002383
2.54	3.40E+07	116.30	0.002451
2.03	2.72E+07	76.98	0.002540
1.52	2.04E+07	45.20	0.002660
1.02	1.36E+07	21.78	0.002846
0.51	6.80E+06	6.14	0.003212
0.25	3.40E+06	1.68	0.003653

Froudes Data 1872

Surface Finish: Tin/Varnish

Velocity	Reynolds No.	Skin Friction	C_F
3.30	4.42E+07	202.10	0.002520
3.05	4.08E+07	175.03	0.002558
2.54	3.40E+07	124.26	0.002619
2.03	2.72E+07	82.68	0.002728
1.52	2.04E+07	48.83	0.002874
1.02	1.36E+07	23.21	0.003033
0.51	6.80E+06	6.28	0.003283
0.25	3.40E+06	1.45	0.003157

D. Data for 1ft (0.305m) Plate

Grid Information

Y-Distribution (Blocks 1,2 &3)	: 36 GP 1.08	(0.003m-0.05m)
X-Distribution (Blocks 1 & 3)	: 40 GP 0.92	(0.002m-0.05m)
X-Distribution (Block 2)	: 61 SYM GP 1.06	(0.002m-0.01m)
Total No. Cells	: 5076	

Laminar Flow Results

Differencing: u & v (Quick)

Velocity	Reynolds No.	Skin Friction	C_F	No. It	CPU Time
5.08	1.36E+06	2.27	0.000597	95	1.11E+02
4.06	1.09E+06	1.81	0.000743	95	1.12E+02
3.56	9.52E+05	1.58	0.000847	95	1.12E+02
3.05	8.16E+05	1.34	0.000984	95	1.15E+02
2.54	6.80E+05	1.11	0.001174	95	1.20E+02
2.03	5.44E+05	0.88	0.001454	95	1.16E+02
1.52	4.08E+05	0.65	0.001911	95	1.21E+02
1.02	2.72E+05	0.42	0.002783	95	1.12E+02
0.51	1.36E+05	0.19	0.005090	96	1.14E+02
0.25	6.80E+04	0.08	0.008491	98	1.24E+02

Turbulent Flow Results

Turbulence Model: K-ε

Differencing: u & v (QUICK), K & ε (HYBRID)

Log-Law Constant: 9.793

Velocity	Reynolds No.	Skin Friction	C_F	No. It	CPU Time
5.08	1.36E+06	17.76	0.004678	195	3.35E+02
4.06	1.09E+06	11.86	0.004883	234	4.08E+02
3.56	9.52E+05	9.32	0.005011	233	4.02E+02
3.05	8.16E+05	7.06	0.005165	125	2.23E+02
2.54	6.80E+05	5.08	0.005357	125	2.19E+02
2.03	5.44E+05	3.40	0.005605	125	2.15E+02
1.52	4.08E+05	2.03	0.005954	124	2.17E+02
1.02	2.72E+05	0.99	0.006498	110	1.94E+02
0.51	1.36E+05	0.29	0.007634	112	1.83E+02
0.25	6.80E+04	0.09	0.009144	257	4.23E+02

Turbulent Flow Results

Turbulence Model: K-ε RNG

Differencing: u & v (QUICK), K & ε (HYBRID)

Log-Law Constant: 9.793

Velocity	Reynolds No.	Skin Friction	C_F	No. It	CPU Time
5.08	1.36E+06	17.72	0.004669	195	3.45E+02
4.06	1.09E+06	11.84	0.004873	234	4.00E+02
3.56	9.52E+05	9.30	0.005001	233	4.14E+02
3.05	8.16E+05	7.04	0.005155	125	2.20E+02
2.54	6.80E+05	5.07	0.005345	125	2.21E+02
2.03	5.44E+05	3.40	0.005591	125	2.23E+02
1.52	4.08E+05	2.03	0.005936	124	2.19E+02
1.02	2.72E+05	0.98	0.006478	110	1.99E+02
0.51	1.36E+05	0.29	0.007597	110	2.02E+02
0.25	6.80E+04	0.09	0.009062	245	4.34E+02

ITTC 1957 Model-Ship correlation Line

Velocity	Reynolds No.	Skin Friction	C_F
5.08	1.36E+06	16.66	0.004390
4.06	1.09E+06	11.16	0.004603
3.56	9.52E+05	8.83	0.004738
3.05	8.16E+05	6.71	0.004902
2.54	6.80E+05	4.85	0.005107
2.03	5.44E+05	3.26	0.005375
1.52	4.08E+05	1.96	0.005754
1.02	2.72E+05	0.97	0.006359
0.51	1.36E+05	0.29	0.007639
0.25	6.80E+04	0.09	0.009349

Froudes Data 1872

Surface Finish: Tin

Velocity	Reynolds No.	Skin Friction	C_F
5.08	1.36E+06	11.62	0.003060
4.06	1.09E+06	7.17	0.002950
3.56	9.52E+05	5.44	0.002920
3.05	8.16E+05	3.71	0.002800
2.54	6.80E+05	2.47	0.002603
2.03	5.44E+05	1.61	0.002640
1.52	4.08E+05	0.96	0.002822

Surface Finish: Varnish

Velocity	Reynolds No.	Skin Friction	C_F
5.08	1.36E+06	16.43	0.004329
4.06	1.09E+06	10.87	0.004476
3.56	9.52E+05	8.40	0.004517
3.05	8.16E+05	6.18	0.004515
2.54	6.80E+05	4.45	0.004687
2.03	5.44E+05	2.96	0.004869
1.52	4.08E+05	1.80	0.005272

E. Data for 16ft (4.877m) Plate

Grid Information

Y-Distribution (Blocks 1,2 &3)	: 67 GP 1.09	(0.0028m-0.80m)
X-Distribution (Blocks 1 & 3)	: 40 GP 0.92	(0.032m-0.80m)
X-Distribution (Block 2)	: 61 SYM GP 1.06	(0.032m-0.16m)
Total No. Cells	: 9447	

Turbulent Flow Results

Turbulence Model: K-ε

Differencing: u & v (QUICK), K & ε (HYBRID)

Log-Law Constant: 9.793

Velocity	Reynolds No.	Skin Friction	C_F	No. It	CPU Time
5.08	2.18E+07	171.34	0.002821	440	1.80E+03
4.06	1.74E+07	113.50	0.002920	435	1.77E+03
3.56	1.52E+07	88.74	0.002982	437	1.90E+03
3.05	1.31E+07	66.80	0.003055	438	1.91E+03
2.54	1.09E+07	47.78	0.003147	438	1.93E+03
2.03	8.70E+06	31.74	0.003266	432	1.93E+03
1.52	6.53E+06	18.75	0.003430	419	1.66E+03
1.02	4.35E+06	8.96	0.003687	397	1.58E+03
0.51	2.18E+06	2.56	0.004218	422	1.70E+03
0.25	1.09E+06	0.78	0.005119	510	2.17E+03

ITTC 1957 Model-Ship correlation Line

Velocity	Reynolds No.	Skin Friction	C_F
5.08	2.18E+07	159.92	0.002633
4.06	1.74E+07	105.95	0.002731
3.56	1.52E+07	83.28	0.002792
3.05	1.31E+07	62.75	0.002866
2.54	1.09E+07	44.90	0.002957
2.03	8.70E+06	29.81	0.003074
1.52	6.53E+06	17.60	0.003236
1.02	4.35E+06	8.54	0.003486
0.51	2.18E+06	2.44	0.003986
0.25	1.09E+06	0.68	0.004603

Froudes Data 1872

Surface Finish: Tin/Varnish

Velocity	Reynolds No.	Skin Friction	C_F
4.06	1.74E+07	112.17	0.002891
3.56	1.52E+07	88.00	0.002950
3.05	1.31E+07	65.76	0.003003
2.54	1.09E+07	46.90	0.003089
2.03	8.70E+06	30.94	0.003191
1.52	6.53E+06	18.20	0.003347
1.02	4.35E+06	8.80	0.003594

F. Data for 500ft (152.4m) Plate

Grid Information

Y-Distribution (Blocks 1,2 &3)	: 74 GP 1.09	(0.050m-25.0m)
X-Distribution (Blocks 1 & 3)	: 40 GP 0.92	(1.0m-25.0m)
X-Distribution (Block 2)	: 61 SYM GP 1.06	(1.0m-5.1m)
Total No. Cells	: 10434	

Turbulent Flow Results

Turbulence Model: K-ε

Differencing: u & v (QUICK), K & ε (HYBRID)

Log-Law Constant: 9.793

Velocity	Reynolds No.	Skin Friction	C_F	No. It	CPU Time
5.08	6.80E+08	3338.00	0.001759	912	4.28E+03
4.06	5.44E+08	2194.00	0.001806	946	4.49E+03
3.56	4.76E+08	1708.40	0.001837	965	4.48E+03
3.05	4.08E+08	1279.40	0.001872	987	4.57E+03
2.54	3.40E+08	909.00	0.001916	1010	4.82E+03
2.03	2.72E+08	598.60	0.001971	1029	4.51E+03
1.52	2.04E+08	349.40	0.002045	1070	4.69E+03
1.02	1.36E+08	163.80	0.002158	1108	4.83E+03
0.51	6.80E+07	45.02	0.002372	1154	4.91E+03
0.25	3.40E+07	12.44	0.002621	1086	4.77E+03

ITTC 1957 Model-Ship correlation Line

Velocity	Reynolds No.	Skin Friction	C_F
5.08	6.80E+08	3050.11	0.001607
4.06	5.44E+08	2004.00	0.001653
3.56	4.76E+08	1567.83	0.001682
3.05	4.08E+08	1174.06	0.001716
2.54	3.40E+08	834.18	0.001758
2.03	2.72E+08	549.19	0.001812
1.52	2.04E+08	320.14	0.001884
1.02	1.36E+08	152.58	0.001994
0.51	6.80E+07	42.18	0.002205
0.25	3.40E+07	11.27	0.002451

G. Data for 1000ft (304.8m) Plate

Grid Information

Y-Distribution (Blocks 1,2 &3)	: 74 GP 1.09	(0.050m-50.0m)
X-Distribution (Blocks 1 & 3)	: 40 GP 0.92	(2.0m-50.0m)
X-Distribution (Block 2)	: 61 SYM GP 1.06	(2.0m-10.0m)
Total No. Cells	: 10434	

Turbulent Flow Results

Turbulence Model: K-ε

Differencing: u & v (QUICK), K & ε (HYBRID)

Log-Law Constant: 9.793

Velocity	Reynolds No.	Skin Friction	C_F	No. It	CPU Time
5.08	1.36E+09	6144.00	0.001619	819	4.01E+03
4.06	1.09E+09	4038.00	0.001662	843	4.22E+03
3.56	9.52E+08	3140.00	0.001688	859	4.29E+03
3.05	8.16E+08	2350.00	0.001720	875	4.36E+03
2.54	6.80E+08	1668.60	0.001758	902	4.35E+03
2.03	5.44E+08	1097.40	0.001807	936	4.47E+03
1.52	4.08E+08	639.80	0.001873	979	4.64E+03
1.02	2.72E+08	299.20	0.001970	1044	4.92E+03
0.51	1.36E+08	81.90	0.002158	1133	4.80E+03

ITTC 1957 Model-Ship correlation Line

Velocity	Reynolds No.	Skin Friction	C_F
5.08	1.36E+09	6145.77	0.001474
4.06	1.09E+09	4029.82	0.001515
3.56	9.52E+08	3146.84	0.001540
3.05	8.16E+08	2353.59	0.001570
2.54	6.80E+08	1668.36	0.001607
2.03	5.44E+08	1095.35	0.001653
1.52	4.08E+08	636.54	0.001716
1.02	2.72E+08	301.49	0.001812
0.51	1.36E+08	82.57	0.001994